Thermal nonequilibrium in partially ionized atomic oxygen

W. H. Soon and J. A. Kunc
Department of Aerospace Engineering and Department of Physics, University of Southern California, Los Angeles, California 90089-1191
(Received 5 September 1989)

A stationary, nonlinear collisional-radiative model for high-temperature atomic oxygen is presented. Populations of electrons, ions and excited atoms and intensities of spectral, continuum, and dielectronic recombination lines are calculated in a wide range of conditions (11 000 K $\leq T_e \leq$ 15 000 K, $10^{10} \leq N_t \leq 10^{18}$ cm^{-3}). Transport of radiation is included by coupling the rate equations for production of the electrons, ions, and excited atoms with the concept of the escape factors that are not constant but dependent upon plasma conditions. The calculated total continuum emission is in good agreement with existing measurements.

I. INTRODUCTION

We investigate in this work collisional and radiative processes in stationary, uniform atomic oxygen at electron temperatures 11 000 K $\lesssim T_e \lesssim$ 15 000 K. In our previous paper,[1] referred to as paper I, a stationary collisional-radiative model was formulated and solved for atomic nitrogen plasma. We refer the reader to paper I for a detail discussion on the development, assumptions, and method of solution of the model.

Since this paper is based upon the same basic assumptions as in paper I, a brief review is in order. We assume in what follows that (1) the plasma is spatially uniform and electrically neutral, (2) the electron-atom and photon-atom inelastic collisions dominate nonequilibrium properties of the plasma, (3) the electron energy distribution is Maxwellian, and (4) nonequilibrium is caused by the escape of radiation from the plasma. Because of the importance of spectral and continuum lines in diagnostics of hot gases, a significant part of this work has been devoted to obtain the best possible cross sections and Einstein coefficients which are used in the model rates equations. The solution of the collisional-radiative model has established the following stationary properties of the high-temperature atomic oxygen: (a) production of electrons, ions (negative and positive), and excited atoms as a function of plasma temperature and density, (b) deviation of the electrons, ions, and excited atom populations from thermal equilibrium, (c) intensities of spectral, continuum, and dielectronic recombination lines, (d) contribution of photoabsorption to the nonequilibrium plasma properties, and (e) relaxation times for the excited atoms.

II. ATOMIC MODEL

The electronic energy structure assumed for atomic oxygen is shown in Fig. 1. All the atomic levels, except the levels $i=2$ and 3, have the ground ionic terms $2p^3\,{}^4S^\circ$ as their atomic "cores." The ionic term $2p^3\,{}^2D^\circ$ and $2p^3\,2P^\circ$ were selected as the cores for $i=2$ ($2p^4\,{}^1D$) and $i=3$ ($2p^4\,{}^1S$) levels, respectively.

It should be added that the ten-level model gives a reliable prediction of the electron and the excited atom densities and the production of radiation in plasmas considered here. Comparison with an eight-level model results shows only small differences in nonequilibrium properties of the plasma.

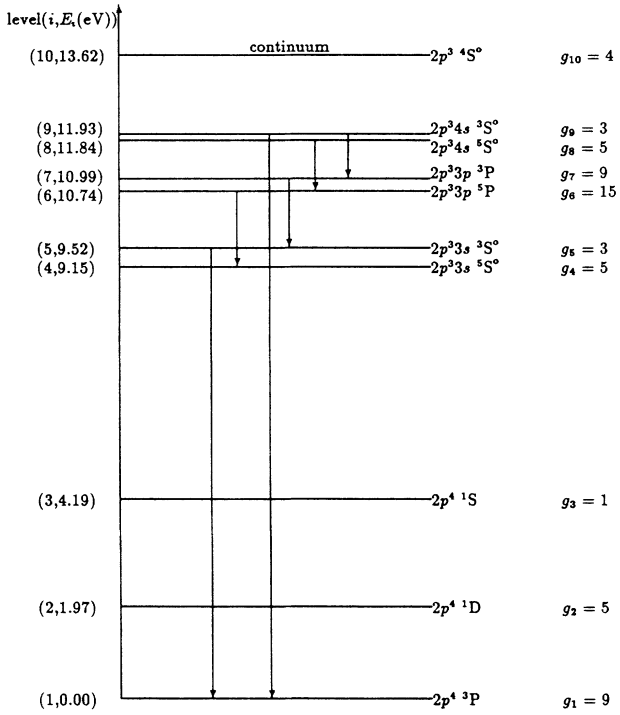

FIG. 1. Energy levels of the oxygen atom assumed in the present work. Energies E_i of the levels are measured with respect to the ground state ($i=1$) and g_i denotes the statistical weight of the ith level. The arrows indicate the electric dipole-allowed transitions.

III. PRODUCTION OF NEGATIVE IONS

We consider only the ground-state [$O^-(^2P)$] ions since the excited negative oxygen ions are not stable. The *total* cross sections for the radiative and electron-impact detachment processes are available in literature.[2,3] These processes are defined, respectively, as

$$h\nu + O^-(^2P) \rightarrow e + O\left[\sum(i)\right], \quad [\eta_{1i}^{\text{tot}}] \tag{1}$$

and

$$e + O^-(^2P) \rightarrow e + O\left[\sum(i)\right] + e, \quad [\mu_{1i}^{\text{tot}}] \tag{2}$$

where $O[\sum(i)]$ indicates that the oxygen atom can be in all possible electronic levels and the symbols in the square brackets denote the corresponding rate coefficients.

The detail balance relationship that relates the *total* cross section for attachment to the *total* cross section for the detachment is not available. Therefore we consider below the attachment processes involving only the ground atomic state $O(^3P)$, that is,

$$e + O(^3P) \rightarrow O^-(^2P) + h\nu, \quad [\gamma_{11}] \tag{3}$$

$$e + O(^3P) + e \rightarrow O^-(^2P) + e, \quad [\omega_{11}] \tag{4}$$

where the symbols in the square brackets denote the corresponding attachment rate coefficients.

The cross section for the radiative attachment with the atom in the ground-state [process (3)] can be obtained from the principle of detail balance[4] as

$$\sigma_{h\nu,\text{att}}^{O(^3P)}(\varepsilon) = \frac{g_-}{g_e g_1}\left[\frac{h\nu}{c}\right]^2 \frac{1}{m_e \varepsilon}\sigma_{h\nu,\text{det}}^{O(^3P)}(\nu) , \tag{5}$$

where g_-, g_e, and g_1 are statistical weights for the negative ion, electron, and the ground atomic state, respectively, ε is the electron energy, $h\nu$, is equal to $\varepsilon + U_-$ (U_- is the electron affinity of the ground-state atom), $\sigma_{h\nu,\text{det}}^{O(^3P)}(\nu)$ is the cross section for the photodetachment process [reverse of the process (3)] that leaves atom in its ground state. The low-energy part ($h\nu \leq 3.5$ eV) of the photodetachment cross section can be obtained from the experimental measurements of Branscomb,[2] while the high-energy part can be taken from the theoretical work of Smith.[5] Subsequently, the rate coefficient γ_{11} for radiative attachment to the ground-state atom is calculated by integrating the cross section (5) over the Maxwellian distribution; the rate is almost independent of T_e within the range of conditions considered in this work.

The three-body attachment rate coefficient ω_{11} can be obtained from the detail balance principle as

$$\omega_{11} = \frac{g_-}{g_e g_1}\left[\frac{h^2}{2\pi m_e k T_e}\right]^{3/2} \exp\left[\frac{U_-}{kT_e}\right]\mu_{11} = P_1 \mu_{11} , \tag{6}$$

where μ_{11} is the rate coefficient for the electron-impact detachment to the ground state and it is not available in the literature. However, under the conditions of this work, μ_{11} is close to the *total* detachment rate coefficient μ_{1i}^{tot}. (The latter rate coefficient is calculated by using the *total* detachment cross section measured by Tisone and Branscomb[3]). This is because the cross sections $\sigma_{e,\text{det}}^{O(^3P)}$ and $\sigma_{e,\text{det}}^{\text{tot}}$ are very close to each other up to an electron energy of about 4 eV. The rate coefficients $\mu_{1i}^{\text{tot}}(\approx\mu_{11})$, γ_{11}, and ω_{11} ($\approx\omega_{i1}^{\text{tot}}$) are given in Figs. 2 and 3, respectively.

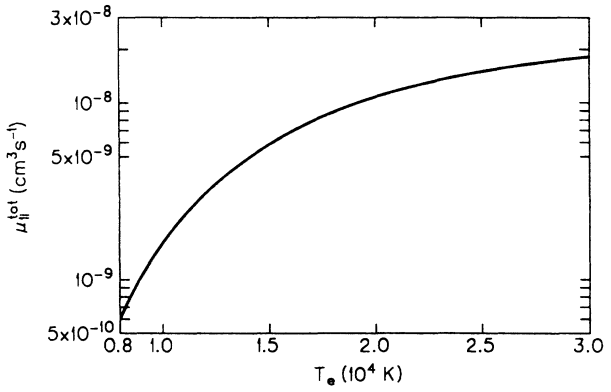

FIG. 2. Total rate coefficient μ_{1i}^{tot} as a function of T_e for the electron-impact detachment of the negative oxygen ion [process (2)].

Another important process depopulating and populating the negative oxygen ions is the mutual neutralization

$$O^-(^2P) + O^+ \rightarrow O(i) + O(j) + \Delta E, \quad [\alpha_{\text{mut}}] \tag{7}$$

and its reverse process

$$O(i) + O(j) + \Delta E \rightarrow O^-(^2P) + O^+, \quad [\alpha_{R_{\text{mut}}}] \tag{8}$$

where we assume that the products of the process (7) are[6] 48% in the $2p^4\,^3P$ ($i=1$) and $2p^3 3p\,^3P$ ($j=7$) states with $\Delta E = 1.16$ eV, 40% in the $2p^4\,^3P$ ($i=1$) and $2p^3 3p\,^5P$ ($j=6$) states with $\Delta E = 1.41$ eV, and 12% in the $2p^4\,^1D$ ($i=2$) and $2p^3 3s\,^5S^\circ$ ($j=4$) states with $\Delta E = 1.04$ eV. The rate coefficient for the mutual neutralization has been measured by Olson, Peterson, and Moseley[7] at temperatures from 300 to 3600 K showing the following tem-

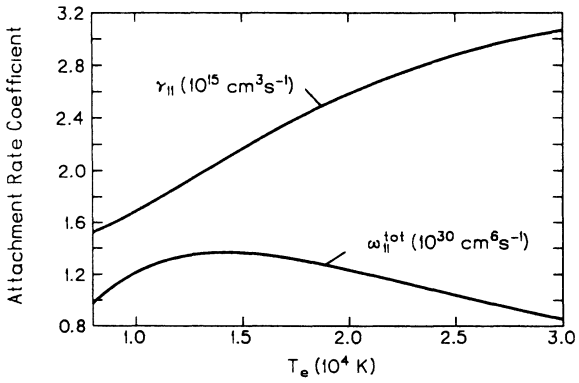

FIG. 3. Rate coefficient γ_{11} for the oxygen atom radiative (two-body) attachment [process (3)] and the total rate coefficient ω_{i1}^{tot} for the electron (three-body) attachement [process (4)].

perature dependence of the rate

$$\alpha_{\text{mut}}=2.8\times10^{-7}\left[\frac{300}{T(\text{K})}\right]^{1/2}\text{cm}^3\,\text{s}^{-1}\,, \tag{9}$$

where the ionic temperature T is assumed to be equal to the atomic temperature. It should be added that the rate coefficient given in Eq. (9) agrees to within a factor of 2 with the complex potential model calculations of Hickman.[8]

The process (8) can be important at temperatures considered here because ΔE is close to the average energy of the gas particles. The rate coefficient $\alpha_{R_{\text{mut}}}$ for the process can be obtained from balancing the processes (7) and (8) under collision dominated, high-density, conditions. Then,

$$\alpha_{R_{\text{mut}}}=\frac{N_-^S N_+^S \alpha_{\text{mut}}}{0.48N_7^S N_1^S+0.4N_6^S N_1^S+0.12N_4^S N_2^S}\,, \tag{10}$$

where the populations of the negative ions (N_-^S), positive ions (N_+^S) and atoms (N_i^S) are calculated from the corresponding Saha relationships.

IV. COLLISIONAL-RADIATIVE MODEL

Taking the attachment, detachment, and mutual neutralization processes into account, one can write the following rate equation for the production of the ground-state negative ions:

$$\frac{\partial N_-}{\partial t}=N_e N_1(\gamma_{11}+N_e\omega_{11})+(0.48N_7N_1+0.4N_6N_1+0.12N_4N_2)\alpha_{R_{\text{mut}}}-(N_{h\nu}N_-\eta_{1i}^{\text{tot}}+N_eN_-\mu_{1i}^{\text{tot}}+N_-N_+\alpha_{\text{mut}})\,, \tag{11}$$

where N_- and $N_{h\nu}$ are negative ion and photon densities, respectively. The plasma is assumed to be transparent to the continuum photons produced in the radiative attachment process.

Similarly, the rate equation for production of electrons is

$$\frac{\partial N_e}{\partial t}=\sum_i N_eN_iS_{ic}-\sum_i N_eN_eN_+\beta_{ci}-\sum_i N_eN_+(\alpha_{ci}^R\kappa_{ci}+\alpha_i^D\langle\kappa_{ai}\rangle)+N_{h\nu}N_-\eta_{1i}^{\text{tot}}+N_eN_-\mu_{1i}^{\text{tot}}-N_eN_1(\gamma_{11}+N_e\omega_{11})\,, \tag{12}$$

where S_{ic} is the electron-impact rate coefficient for ionization of atom excited to the ith level; α_{ci}^R and β_{ci} are rate coefficients for radiative and three-body recombination, respectively, producing an atom excited to the ith level; α_i^D is the effective dielectronic recombination rate coefficient for dielectronic transitions to the $i=1$ and 4 "terminating" levels (see discussion below); and $\langle\kappa_{ai}\rangle$ and κ_{ci} are the radiation escape factor for dielectronic and free-bound radiation, respectively.

The rate equation for the production of the excited atoms should include the attachment, detachment, and mutual neutralization processes involving atoms excited to particular electronic levels. Then, the production of the excited atoms can be given by

$$\begin{aligned}\frac{\partial N_i}{\partial t}=&\sum_{k(<i)}N_eN_kC_{ki}+\sum_{j(>i)}N_eN_jR_{ji}+\sum_{j(>i)}N_jA_{ji}\kappa_{ji}+N_eN_+(\alpha_{ci}^R\kappa_{ci}+\alpha_i^D\langle\kappa_{ai}\rangle+N_e\beta_{ci})\\&-N_i\left[\sum_{j(>i)}N_eC_{ij}+\sum_{k(<i)}N_eR_{ik}+\sum_{k(<i)}A_{ik}\kappa_{ik}+N_eS_{ic}\right]\\&+N_{h\nu}N_-\eta_{1i}+N_eN_-\mu_{1i}-N_eN_i(\gamma_{i1}+N_e\omega_{i1})\\&+\{0.48[\delta_7(i)+\delta_1(i)]+0.4[\delta_6(i)+\delta_1(i)]+0.12[\delta_2(i)+\delta_4(i)]\}N_-N_+\alpha_{\text{mut}}\\&-\{0.48N_7N_1[\delta_7(i)+\delta_1(i)]+0.4N_6N_1[\delta_6(i)+\delta_1(i)]+0.12N_4N_2[\delta_2(i)+\delta_4(i)]\}\alpha_{R_{\text{mut}}}\,,\end{aligned} \tag{13}$$

$$\delta_k(i)=\begin{cases}1, & \text{if } k=i\\0, & \text{otherwise}\end{cases}$$

where C_{ij} and R_{ji} are the rate coefficients for the electron-impact excitation and deexcitation, respectively; A_{ji} and κ_{ji} are the transition probability (the Einstein coefficient) and the radiation escape factor for the $(j\rightarrow i)$ radiative transition, respectively; η_{1i} and μ_{1i} are rate coefficients for the following radiative and electron-impact detachment processes:

$$h\nu+\text{O}^-(^2P)\rightarrow e+\text{O}(i),\quad[\eta_{1i}] \tag{14}$$

and

$$e+\text{O}^-(^2P)\rightarrow e+\text{O}(i)+e,\quad[\mu_{1i}] \tag{15}$$

and γ_{i1} and ω_{i1} are rate coefficients for the radiative and electron-impact attachment processes

$$e+\text{O}(i)\rightarrow\text{O}^-(^2P)+h\nu,\quad[\gamma_{i1}] \tag{16}$$

and

$$e+\mathrm{O}(i)+e\rightarrow \mathrm{O}^-(^2P)+e, \quad [\omega_{i1}] . \tag{17}$$

In the present study, only the attachment and detachment processes involving the ground-state atom is taken into consideration.

Neglecting the small radiative detachment term in Eq. (11), one obtains for the steady state

$$\frac{N_-}{N_e N_1}=K\left[\frac{g_-}{g_e g_1}\left[\frac{h^2}{2\pi m_e kT_e}\right]^{3/2}\exp\left[\frac{U_-}{kT_e}\right]\right]=KP_1 , \tag{18}$$

where the factor $K=N_-/N_-^S$, a measure of deviation of the negative ion population from Saha equilibrium, is

$$K=\frac{(\gamma_{11}/N_e)+\omega_{11}(0.48\rho_7 G_7+0.4\rho_6 G_6+0.12\rho_4 G_4 B_2 F_2)\alpha_{R_{\mathrm{mut}}}}{\omega_{11}+P_1\alpha_{\mathrm{mut}}} , \tag{19}$$

$$G_i=\frac{g_i}{g_e g_+}\left[\frac{h_2}{2\pi m_e kT_e}\right]^{3/2}\exp\left[\frac{U_i}{kT_e}\right] , \tag{20}$$

$$F_i=\frac{g_i}{g_1}\exp\left[-\frac{E_i-E_1}{kT_e}\right] , \tag{21}$$

the nonequilibrium Saha factor ρ_i is defined as

$$\rho_i=N_i/N_i^S , \tag{22}$$

and the nonequilibrium Boltzmann factor B_i is defined below.

The steady-state density of atoms excited to the ith level can be given in a convenient Boltzmann-like form

$$\frac{N_i}{N_1}=B_i F_i , \tag{23}$$

where $B_i=B_i^N/B_i^D$ with

$$\begin{aligned}B_i^N=&N_e\sum_{k(<i)}B_k F_k C_{ki}+N_e\sum_{j(>i)}B_j F_j R_{ji}+\sum_{j(>i)}B_j F_j A_{ji}\kappa_{ji}\\&+(H_{n_{\max}}/G_1)(\alpha_{ci}^R\kappa_{ci}+\alpha_i^D\langle\kappa_{ai}\rangle+N_e\beta_{ci})+(N_e K P_1)N_e\mu_{1i}\\&+\{0.48[\delta_7(i)+\delta_1(i)]+0.4[\delta_6(i)+\delta_1(i)]+0.12[\delta_2(i)+\delta_4(i)]\}(N_e K P_1)N_+\alpha_{\mathrm{mut}} ,\end{aligned} \tag{24}$$

$$\begin{aligned}B_i^D=F_i\Bigg[&N_e\left[\sum_{k(<i)}R_{ik}+\sum_{j(>i)}C_{ij}+S_{ic}\right]+\sum_{k(<i)}A_{ik}\kappa_{ik}\\&+[0.48N_7N_1\Delta A(i)+0.4N_6N_1\Delta B(i)+0.12N_4N_2\Delta C(i)]\alpha_{R_{\mathrm{mut}}}\Bigg] ,\end{aligned} \tag{25}$$

$\Delta A(i)=1/N_i$, if $i=1$ or 7, 0 otherwise

$\Delta B(i)=1/N_i$, if $i=1$ or 6, 0 otherwise

$\Delta C(i)=1/N_i$, if $i=2$ or 4, 0 otherwise .

Similarly, the steady-state production of electrons can be expressed in a Saha-like form

$$\frac{N_+N_e}{N_1}=H_{n_{\max}}\left[\frac{g_e g_+}{g_1}\left[\frac{2\pi m_e kT_e}{h^2}\right]^{3/2}\exp\left[-\frac{U_1}{kT_e}\right]\right]=\frac{H_{n_{\max}}}{G_1} , \tag{26}$$

where

$$H_{n_{\max}}=\frac{\sum_{i=1}^{n_{\max}}B_i\beta_{ci}+(N_e K G_1)\omega_{11}}{\sum_{i=1}^{n_{\max}}[\beta_{ci}+(\alpha_{ci}^R\kappa_{ci}+\alpha_i^D\langle\kappa_{ai}\rangle)/N_e]+(N_1/N_+N_e)(\gamma_{11}+N_e\omega_{11})} . \tag{27}$$

The steady-state solution of Eqs. (11)–(13) for given T_e and N_t can be obtained, assuming charge neutrality ($N_+=N_e+N_-$), by iterations with the initial guess of B_i obtained in the way discussed in paper I.

V. EXCITATION CROSS SECTIONS AND RATE COEFFICIENTS

The main theoretical approach used here for determination of the electron-impact cross sections and rate

coefficients for atomic excitation is the one formulated by Vainshtein and his colleagues.[1,9,10] The principle of detailed balance is applied to obtain the deexcitation rate coefficients since the electron energy distribution is Maxwellian.

As discussed in paper I the Vainshtein approach seems to have acceptable accuracy in the cases of atomic systems such as nitrogen and oxygen. More accurate general approaches have been formulated (e.g., close coupling and R-matrix method; see discussion in paper I), but they are very complex, and people and time intensive, and they were performed only for a very limited number of transitions in a few atomic systems (those related to the electron-oxygen atom collisions are included in this work). Therefore use of the approximate methods such as the Vainshtein theory is necessary in studies of collisional-radiative nonequilibrium in partially ionized plasmas (see also the discussion in Sec. XIII).

A number of reliable measurements of cross sections for several electron-impact excitation transitions have been reported recently.[11–17] All these cross sections are assumed in the present work.

A. Electron-impact excitation with $|\Delta S|=0$

1. Experimental cross sections

We use here the recently measured cross sections[13,14] for the $1\rightarrow5$ and $1\rightarrow7$ transitions in oxygen atom. Comparison of the measured $1\rightarrow5$ cross section with other measurements,[17] and with Julienne and Davis's,[18] Smith's[19] and Rountree and co-worker's[20,21] calculations gives an acceptable agreement. The $1\rightarrow7$ cross section used in this work agrees well with experimental data of Zipf (see Ref. 13) and the close coupling calculations of Smith.[19]

2. $2\rightarrow3$ transition

The cross section for the $2\rightarrow3$ transition was taken from the close-coupling calculations of Henry, Burke, and Sinfailam.[22] This cross section agrees very well with the cross sections of Lan *et al.*[23] and Thomas and Nesbet,[24] and it seems to be more accurate than the cross sections obtained earlier by Smith *et al.*[25,26] and Seaton.[27]

3. $1\rightarrow9$ transition

The close-coupling cross sections of Smith[19] for the electron-impact $1\rightarrow9$ transition is used in the present calculations. This choice results from the fact that the approach of Smith gives cross sections that are in good agreement with results of other calculations,[18,28] and with the recent measurements for the $1\rightarrow5$ and $1\rightarrow7$ transitions in atomic oxygen.[11,13,14,17]

4. Other transitions

All $|\Delta S|=0$ transitions, other than those discussed above, are calculated by using the Vainshtein approach,[9] which is based on the Born-Coulomb approximation (see paper I). Vainshtein's rate coefficients for these transitions can be fitted to the following expression:

$$C_{ij}(\beta)=10^{-8}\left[\frac{\mathcal{R}U_j}{\Delta E_{ij}U_i}\right]^{3/2}\frac{Q_k}{2l_i+1}\times\exp(-\beta)G_k(\beta)\ \mathrm{cm^3\,s^{-1}}\ , \tag{28}$$

where $k=|l_j-l_i|$ and the function $G_k(\beta)$ is

$$G_k(\beta)=\frac{A\sqrt{\beta(\beta+1)}}{\beta+\chi}\ln(16+1/\beta),\quad \text{for } k=1 \tag{29}$$

$$G_k(\beta)=\frac{A\sqrt{\beta(\beta+1)}}{\beta+\chi},\quad \text{for } k\neq1 \tag{30}$$

where

$$\beta=\frac{\Delta E_{ij}}{kT_e}\ , \tag{31}$$

ΔE_{ij} is the energy gap of the $i\rightarrow j$ transition, $\mathcal{R}$ is the Rydberg energy, and U_i and l_i are the ionization potential and orbital angular momentum quantum number of the lower level i, respectively. The parameters A and χ and the angular factors Q_k are given in Table I.

B. Electron-impact excitation with $|\Delta S|=1$

1. $1\rightarrow2$, $1\rightarrow3$, $1\rightarrow4$, and $1\rightarrow6$ transitions

The electron-impact cross sections for these transitions are taken from measurements of Doering and coworkers.[11–13] The measured cross sections for the $1\rightarrow2$ and $1\rightarrow3$ transitions agree well with experimental data of Shyn and co-workers,[29,30] and with calculated cross sections of Henry, Burke, and Sinfailam,[22] Lan *et al.*,[23] and Thomas and Nesbet.[24]

The cross section for the $1\rightarrow4$ transition is in good agreement with theoretical results of Smith[19] and Julienne and Davis.[18] The cross section for the $1\rightarrow6$ transition shows an acceptable agreement with theoretical cross section of Sawada and Ganas.[28]

2. Other transitions

The cross sections for all $|\Delta S|=1$ intercombinative transitions, except the few cases mentioned above, are obtained from the Vainshtein approach when only pure exchange is considered. Then, the rate coefficients for electron-impact excitation can be fitted to the following expression:

$$C''_{ij}(\beta)=10^{-8}\left[\frac{\mathcal{R}U_j}{\Delta E_{ij}U_i}\right]^{3/2}\frac{Q''}{2l_i+1}\times\exp(-\beta)G''(\beta)\ \mathrm{cm^3\,s^{-1}}\ , \tag{32}$$

where the function $G''(\beta)$ is

$$G''(\beta)=\frac{A''\beta}{(\beta+\chi'')}\left[\frac{\beta}{\beta+1}\right]^{1/2}\ , \tag{33}$$

and the parameters A'' and χ'' and the angular factors Q'' are given in Table I.

TABLE I. Parameters in the rate coefficients for electron-impact excitation of atomic oxygen. The designation of the inner shells $1s^2 2s^2$ is omitted in electronic configuration in every table.

$i \rightarrow j$	Transition	$\lvert\Delta S\rvert$	Q_k	A	χ
1→8	$2p^4\,{}^3P \rightarrow 2p^3 4s\,{}^5S^\circ$	1	$\frac{5}{6}$	1.39	0.04
2→5	$2p^4\,{}^1D \rightarrow 2p^3 3s\,{}^3S^\circ$	1	$\frac{9}{4}$	1.277	0.038
2→7	$2p^4\,{}^1D \rightarrow 2p^3 3p\,{}^3P$	1	$\frac{9}{4}$	4.899	0.353
2→9	$2p^4\,{}^1D \rightarrow 2p^3 4s\,{}^3S^\circ$	1	$\frac{9}{4}$	1.4044	0.04
3→5	$2p^4\,{}^1S \rightarrow 2p^3 3s\,{}^3S^\circ$	1	3	1.239	0.056
3→7	$2p^4\,{}^1S \rightarrow 2p^3 3p\,{}^3P$	1	3	24.793	0.596
3→9	$2p^4\,{}^1S \rightarrow 2p^3 4s\,{}^3S^\circ$	1	3	0.91	0.04
4→5	$2p^3 3s\,{}^5S^\circ \rightarrow 2p^3 3s\,{}^3S^\circ$	1	$\frac{3}{8}$	1.415	0.0072
4→6	$2p^3 3s\,{}^5S^\circ \rightarrow 2p^3 3p\,{}^5P$	0	1	5.586	0.6538
4→7	$2p^3 3s\,{}^5S^\circ \rightarrow 2p^3 3p\,{}^3P$	1	$\frac{3}{8}$	15.889	1.676
4→8	$2p^3 3s\,{}^5S^\circ \rightarrow 2p^3 4s\,{}^5S^\circ$	0	1	3.288	1.188
4→9	$2p^3 3s\,{}^5S^\circ \rightarrow 2p^3 4s\,{}^3S^\circ$	1	$\frac{3}{8}$	0.9968	0.6285
5→6	$2p^3 3s\,{}^3S^\circ \rightarrow 2p^3 3p\,{}^5P$	1	$\frac{5}{8}$	17.897	1.31
5→7	$2p^3 3s\,{}^3S^\circ \rightarrow 2p^3 3p\,{}^3P$	0	1	5.491	0.609
5→8	$2p^3 3s\,{}^3S^\circ \rightarrow 2p^3 4s\,{}^5S^\circ$	1	$\frac{5}{8}$	4.48	1.106
5→9	$2p^3 3s\,{}^3S^\circ \rightarrow 2p^3 4s\,{}^3S^\circ$	0	1	3.092	1.131
6→7	$2p^3 3p\,{}^5P \rightarrow 2p^3 3p\,{}^3P$	1	$\frac{3}{8}$	7.767	0.822
6→8	$2p^3 3p\,{}^5P \rightarrow 2p^3 4s\,{}^5S^\circ$	0	1	1.041	0.27
6→9	$2p^3 3p\,{}^5P \rightarrow 2p^3 4s\,{}^3S^\circ$	1	$\frac{3}{8}$	1.072	0.623
7→8	$2p^3 3p\,{}^3P \rightarrow 2p^3 4s\,{}^5S^\circ$	1	$\frac{5}{8}$	3.338	1.585
7→9	$2p^3 3p\,{}^3P \rightarrow 2p^3 4s\,{}^3S^\circ$	0	1	1.179	0.287
8→9	$2p^3 4s\,{}^5S^\circ \rightarrow 2p^3 4s\,{}^3S^\circ$	1	$\frac{3}{8}$	2.432	0.0008

C. "Difficult" transitions

The term "difficult" is used here to denote the electron-impact transitions involving excitation of two atomic electrons (all the $|\Delta S|=2$ transitions). We calculate the cross sections for the transitions using the quantum-classical formulation of the binary-encounter approximation.[31] The corresponding cross section for atomic excitation from a lower level i to an upper level j is

$$\sigma_{\rm exc}(\varepsilon)=\frac{\pi e^4}{\varepsilon+2U_i}\left[0.924\left[\frac{1}{\varepsilon+U_i-\Delta E_{ij+1}}-\frac{1}{\varepsilon+U_i-\Delta E_{ij}}\right]+\frac{2U_i}{3}\left[\frac{1}{(\varepsilon+U_i-\Delta E_{ij+1})^2}-\frac{1}{(\varepsilon+U_i-\Delta E_{ij})^2}\right]\right], \quad (34)$$

where ΔE_{ij+1} is to be replaced by ε when $\Delta E_{ij}\le\varepsilon<\Delta E_{ij+1}$ (see paper I).

VI. IONIZATION CROSS SECTIONS AND RATE COEFFICIENTS

A. Experimental cross sections

The cross section used in this work for the electron-impact ionization from the atomic ground state is that measured by Brook, Harrison, and Smith.[32] Their cross section is very close to the cross section measured recently by Zipf.[33]

B. Ionization from the two lowest excited levels

As mentioned before, the $i=2$ and 3 levels of oxygen atom do not couple with the ionic ground state. In the plasmas considered here, the density of the ground-state ions is much greater than the densities of the excited ions. Therefore we neglect in our calculations the three-body recombination from these excited ionic levels to the $i=2$ and 3 atomic levels. However, we include the electron-impact ionization of the two atomic levels (with final ionic states $2p^3\,{}^2D^\circ$ and $2p^3\,{}^2P^\circ$, respectively). In other words, we assume that the contribution of the recombination to production of the $i=2$ and 3 atomic levels can be neglected, in the rate equations (12) and (13), whereas the contribution of the collisional ionization from these two atomic levels can be of some importance (mainly because of the relatively high densities of these two atomic levels).

The $i=2$ and 3 atomic levels belong to the same electronic shell as the atomic ground state. Therefore we use for these levels the same constants A and χ as those for the ground state; A and χ are equal to 30.52 and 4, respectively. The constants were obtained from a numerical fitting of the ionization rate coefficient for the ground state (obtained from the cross section measured by Brook, Harrison, and Smith[32]) to the Vainshtein expression

$$S_{ic}(\beta)=10^{-8}\left[\frac{\mathcal{R}}{U_i}\right]^{3/2}\frac{Q_i}{2l_i+1}\times\exp(-\beta)G_i(\beta)\ \mathrm{cm^3\,s^{-1}}\ , \tag{35}$$

where the angular factors Q_i are $\frac{4}{3}$, 3, and 4 for the levels $i=1$, 2, and 3, respectively, and

$$G_i(\beta)=\left[\frac{\beta}{\beta+1}\right]^{1/2}\frac{A}{\beta+\chi}\ , \tag{36}$$

$$\beta=\frac{U_i}{kT_e}\ . \tag{37}$$

C. Ionization from the excited levels with $i>3$

The cross sections of Gryzinski and Kunc[34] are used for ionization from the excited levels with $i>3$. Their analytical cross section for the electron-impact ionization is

$$\sigma_{ic}(\varepsilon)=\frac{\pi e^4}{U_i^2}\frac{m}{[(\lambda^2+k_g)^{1/2}+1]^2}\times\left[1+\frac{2}{(\lambda^2+k_g)^{1/2}}+\frac{2}{3}\left[1+\frac{1}{\lambda^2}\right]\right]\times\left[1-\frac{1}{\lambda^2}\right]\ , \tag{38}$$

where m is the number of electrons in the atomic outer shell and U_i is the ionization potential for the atom excited to level i. Here $\lambda^2=\varepsilon/U_i$ and $k_g=W/U_i^s$; U_1^s is the first ionization potential of the outer shell and W is the average binding energy of the electrons in the shell (see paper I). The three-body recombination rate coefficients are obtained from the principle of detail balance.

VII. SPONTANEOUS EMISSION

The probabilities for $j\rightarrow i$ spontaneous transitions involving terms with fine structure are obtained by averaging over the entire multiplet (see paper I).

A. Transitions with $|\Delta S|=0$

The magnetic interaction has negligible contribution to the oscillator strengths for the $|\Delta S|=0$ transitions[35,36] and the assumption of LS coupling is valid.

(i) Electric dipole (E1) lines. The Einstein coefficients for the strong electric dipole lines are available in number of works.[37–44] We selected only the most recent and commonly accepted Einstein coefficients. These coefficients are averaged and the averaged values are used in this work (Table II).

(ii) Electric quadrupole (E2) lines. Some of the $|\Delta S|=0$ transitions considered here (other than the electric dipole lines) are violating the magnetic dipole selection rule. Therefore all such transitions (a total of four transitions listed in Table III) are considered here as the electric quadrupole type. The oscillator strength for the $3\rightarrow 2$ transition in oxygen atom was measured by Omholt[45,46] and also estimated from theoretical considerations[47] (both values are in good agreement with each other). The Einstein coefficients for the other three transitions of this kind can be obtained from general relationship[48]

$$A_{ji}=\frac{32\pi^6\nu_{ji}^5}{5hc^5}|\mu_{ji}^{E2}|^2\ , \tag{39}$$

where the electric quadrupole matrix element μ_{ji}^{E2} is estimated as

$$\mu_{ji}^{E2}=e(R_j^{E2})^2\ , \tag{40}$$

with R_j^{E2} interpreted as the averaged radius of the atom excited to the state j,

$$R_j^{E2}\approx\frac{a_0[n_{\mathrm{eff}}(j)]^2}{Z_{\mathrm{eff}}(j)}\ , \tag{41}$$

n_{eff} and Z_{eff} are the effective principal quantum number of the outershell electrons and the effective charge number of the atomic core, respectively. The quantum number n_{eff} of an atom excited to the jth electronic level is

$$n_{\mathrm{eff}}(j)=\left[\frac{\mathcal{R}}{U_j}\right]^{1/2}\ , \tag{42}$$

where $\mathcal{R}$ is the Rydberg energy and U_j is the ionization potential of the atom. The effective charge number of the level is

$$Z_{\mathrm{eff}}(j)=Z-\xi(j)\ , \tag{43}$$

where Z is the atomic number and $\xi(j)$ is the screening constant for the level. The screening constants are calcu-

TABLE II. Electric dipole ($E1$) lines ($|\Delta S|=0$) in the oxygen atom. λ_{ji}, f_{ij}, and A_{ji} are the line wavelength, absorption oscillator strength, and Einstein's coefficient, respectively.

$j\rightarrow i$	Transition	λ_{ji} (Å)	f_{ij}	A_{ji} (s^{-1})
5→1	$2p^3 3s\ ^3S^\circ\rightarrow 2p^4\ ^3P$	1303.5	1.7×10^{-2}	1.99×10^8
9→1	$2p^3 4s\ ^3S^\circ\rightarrow 2p^4\ ^3P$	1039.2	3.1×10^{-3}	5.67×10^7
6→4	$2p^3 3p\ ^5P\rightarrow 2p^3 3s\ ^5S^\circ$	7773.4	9.5×10^{-1}	3.5×10^7
7→5	$2p^3 3p\ ^3P\rightarrow 2p^3 3s\ ^3S^\circ$	8446.5	9.8×10^{-1}	3.05×10^7
8→6	$2p^3 4s\ ^5S^\circ\rightarrow 2p^3 3p\ ^5P$	11 299.0	1.7×10^{-1}	2.64×10^7
9→7	$2p^3 4s\ ^3S^\circ\rightarrow 2p^3 3p\ ^3P$	13 164.0	1.8×10^{-1}	2.02×10^7

TABLE III. Electric quadrupole ($E2$) lines ($|\Delta S|=0$) in the oxygen atom. λ_{ji}, f_{ij}, and A_{ji} are the line wavelength, absorption oscillator strength, and Einstein's coefficient, respectively.

$j\rightarrow i$	Transition	λ_{ji} (Å)	f_{ij}	A_{ji} (s^{-1})
$7\rightarrow 1$	$2p^3 3p\ ^3P\rightarrow 2p^4\ ^3P$	1129.0	9.3×10^{-6}	4.86×10^{4}
$3\rightarrow 2$	$2p^3 3s\ ^5S^\circ\rightarrow 2p^4\ ^1D$	5577.4	1.1×10^{-9}	1.18
$8\rightarrow 4$	$2p^3 4s\ ^5S^\circ\rightarrow 2p^3 3s\ ^5S^\circ$	4608.9	3.2×10^{-7}	9.90×10^{1}
$9\rightarrow 5$	$2p^3 4s\ ^3S^\circ\rightarrow 2p^3 3s\ ^3S^\circ$	5150.3	2.8×10^{-7}	7.02×10^{1}

lated by modifying the approach of Clementi and Raimondi,[49] which was formulated for the ground-state atoms. We assumed that the screening constant $\xi(j)$ for an optical electron of the excited atom is

$$\xi(j)=\xi'(j=1)-\Delta\xi(j)\ , \tag{44}$$

where $\xi'(j=1)$ is the screening constant for an optical electron in the ground-state atom with the electronic configuration of its outer shell similar to the outershell configuration of the excited atom. $\Delta\xi(j)$ is the reduction of the screening effect due to the difference in the electronic configurations of the inner shells in the excited and in the ground-state atom. $\Delta\xi(j)$ was calculated by superposition of the screening constants for the individual orbitals present in the excited atom but absent in the ground-state atom. The effective charge numbers for the ground-state and excited atoms are summarized in Table IV.

B. Transitions with $|\Delta S|=1$

In this case, both magnetic dipole ($M1$) and electric quadrupole ($E2$) interactions are considered (see Table V). The multiplet-averaged Einstein coefficients A_{ji} for the $2\rightarrow1$ and $3\rightarrow1$ transitions are taken from Ref. 44. The oscillator strengths for $5\rightarrow3$, $5\rightarrow2$, and $4\rightarrow1$ intercombinative transitions are taken from Ref. 35.

A simple approach (paper I), based on the results discussed above and on a survey of oscillator strengths for other intercombinative lines, is used here to estimate the Einstein coefficients for the rest of the $|\Delta S|=1$ transitions. We assume values of $f_{ij}=4.8\times10^{-7}$ for lines with wavelength $\lambda_{ji}\lesssim2500$ Å and of $f_{ij}=7.25\times10^{-12}$ when $\lambda_{ji}>2500$ Å. Using these values, the transition probabilities are obtained from[44]

$$A_{ji}=\frac{6.67\times10^{15}}{\lambda_{ji}^2}\frac{g_i f_{ij}}{g_j}\ , \tag{45}$$

with the wavelength λ_{ji} in angstroms and the transition probability A_{ji} in s^{-1}.

TABLE IV. Effective charge numbers $Z_{\rm eff}$ of the atomic oxygen "core."

Level	$Z_{\rm eff}$
$2p^4\ ^3P$	4.424
$2p^4\ ^1D$	4.424
$2p^4\ ^1S$	4.424
$2p^3 3s\ ^5S^\circ$	2.057
$2p^3 3s\ ^3S^\circ$	2.057
$2p^3 3p\ ^5P$	1.916
$2p^3 3p\ ^3P$	1.916
$2p^3 4s\ ^5S^\circ$	2.295
$2p^3 4s\ ^3S^\circ$	2.295

C. Difficult transitions

This section deals with six atomic transitions with $|\Delta S|=2$. The value of the oscillator strength $f_{ij}=10^{-9}$ was assumed[35] for all the difficult transitions (see Table VI). This seems to be reasonable because high accuracy of these A_{ji} is not a crucial issue; the $j\rightarrow i$ collisional deexcitation (the term $N_j N_e R_{ji}$) always dominate the radiative deexcitation (the term $N_j A_{ji}\kappa_{ji}$) in the collisional-radiative balance.

VIII. DIELECTRONIC RECOMBINATION

Dielectronic recombination is a result of a two-stage process: dielectronic capture (with the reverse process—autoionization) followed by radiative stabilizing transition

$$e+X_p^+\rightarrow X_a\rightarrow X_i+h\nu\ , \tag{46}$$

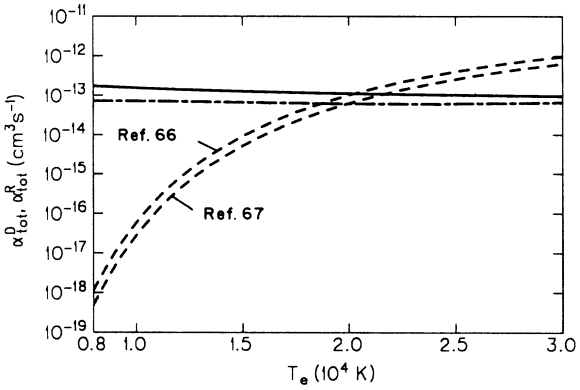

FIG. 4. Comparison of the total dielectronic recombination rate $\alpha^D_{\rm tot}=\sum_{i=1,4}\alpha^D_i$ (dot-dashed line) and the total radiative recombination rate $\alpha^R_{\rm tot}=\sum_{i=1}^{9}\alpha^R_{ci}$ (solid line) of the present work. (BAP) represents the total dielectronic recombination rate of Aldrovandi and Pequignot (Ref. 66) based of the Burgess model neglecting stabilizing transitions of the captured electron. (JSS) represents the total dielectronic recombination rate of Shull and van Steenberg (Ref. 67) based on the Jacobs model also neglecting stabilizing transitions of the captured electron.

TABLE V. Magnetic dipole ($M1$) plus electric quadrupole ($E2$) lines ($|\Delta S|=1$) in the oxygen atom. λ_{ji}, f_{ij}, and A_{ji} are the line wavelength, absorption oscillator strength, and Einstein's coefficient, respectively.

$j\rightarrow i$	Transition	λ_{ji} (Å)	f_{ij}	A_{ji} (s^{-1})
$2\rightarrow 1$	$2p^4\,{}^1D\rightarrow 2p^4\,{}^3P$	6300.2	1.1×10^{-11}	3.39×10^{-3}
$3\rightarrow 1$	$2p^4\,{}^1S\rightarrow 2p^4\,{}^3P$	2972.3	3.3×10^{-12}	2.25×10^{-2}
$4\rightarrow 1$	$2p^3 3s\,{}^5S^\circ\rightarrow 2p^4\,{}^3P$	1355.6	9.0×10^{-7}	5.88×10^{4}
$6\rightarrow 1$	$2p^3 3p\,{}^5P\rightarrow 2p^4\,{}^3P$	1155.2	4.8×10^{-7}	1.45×10^{3}
$8\rightarrow 1$	$2p^3 4s\,{}^5S^\circ\rightarrow 2p^4\,{}^3P$	1048.1	4.8×10^{-7}	5.29×10^{3}
$5\rightarrow 2$	$2p^3 3s\,{}^3S^\circ\rightarrow 2p^4\,{}^1D$	1642.4	5.4×10^{-7}	2.2×10^{3}
$7\rightarrow 2$	$2p^3 3p\,{}^3P\rightarrow 2p^4\,{}^1D$	1375.2	4.8×10^{-7}	9.48×10^{2}
$9\rightarrow 2$	$2p^3 4s\,{}^3S^\circ\rightarrow 2p^4\,{}^1D$	1245.3	4.8×10^{-7}	3.45×10^{3}
$5\rightarrow 3$	$2p^3 3s\,{}^3S^\circ\rightarrow 2p^4\,{}^1S$	2327.3	1.2×10^{-8}	4.93
$7\rightarrow 3$	$2p^3 3p\,{}^3P\rightarrow 2p^4\,{}^1S$	1824.8	4.8×10^{-7}	1.08×10^{2}
$9\rightarrow 3$	$2p^3 4s\,{}^3S^\circ\rightarrow 2p^4\,{}^1S$	1603.0	4.8×10^{-7}	4.19×10^{2}
$5\rightarrow 4$	$2p^3 3s\,{}^3S^\circ\rightarrow 2p^3 3s\,{}^5S^\circ$	33 085.5	7.3×10^{-12}	7.38×10^{-5}
$7\rightarrow 4$	$2p^3 3p\,{}^3P\rightarrow 2p^3 3s\,{}^5S^\circ$	6732.0	7.3×10^{-12}	5.94×10^{-4}
$9\rightarrow 4$	$2p^3 4s\,{}^3S^\circ\rightarrow 2p^3 3s\,{}^5S^\circ$	4456.6	7.3×10^{-12}	4.07×10^{-3}
$6\rightarrow 5$	$2p^3 3p\,{}^5P\rightarrow 2p^3 3s\,{}^3S^\circ$	10 178.1	7.3×10^{-12}	9.36×10^{-5}
$8\rightarrow 5$	$2p^3 4s\,{}^5S^\circ\rightarrow 2p^3 3s\,{}^3S^\circ$	5354.8	7.3×10^{-12}	1.02×10^{-3}
$7\rightarrow 6$	$2p^3 3p\,{}^3P\rightarrow 2p^3 3p\,{}^5P$	49 827.6	7.3×10^{-12}	3.26×10^{-5}
$9\rightarrow 6$	$2p^3 4s\,{}^3S^\circ\rightarrow 2p^3 3p\,{}^5P$	10 426.1	7.3×10^{-12}	2.23×10^{-3}
$8\rightarrow 7$	$2p^3 4s\,{}^5S^\circ\rightarrow 2p^3 3p\,{}^3P$	14 613.7	7.3×10^{-12}	4.09×10^{-4}
$9\rightarrow 8$	$2p^3 4s\,{}^3S^\circ\rightarrow 2p^3 4s\,{}^5S^\circ$	134 859.4	7.3×10^{-12}	4.44×10^{-6}

where p denotes an initial state of the atomic ion X^+, and a and i denote an autoionizing (doubly excited) state and a "true" bound (singly excited) state, respectively, of the atom X.

Nussbaumer and Storey[50,51] showed recently, including the contributions due to the outer electron, that the dielectronic recombination can be important at $T_e<20\,000$ K and that it is much higher than that obtained from the Burgess formula[52,53] (see Fig. 4).

We use here the approach of Nussbaumer and Storey (NS), assuming that the population of the excited ionic levels is much lower than the population of the ground state of the recombining ion [$p=1$ in Eq. (46)]. Since the first excited level ($2p^3\,{}^2D^\circ$) of the O^+ ion is metastable and has the excitation energy about 3 eV, the assumption requires the ratio N_e/N_a to be much less than 1 in the plasmas discussed here. Another assumption of the model is that only radiative transitions satisfying LS coupling are included. At higher plasma densities ($N_e\gtrsim 10^{14}-10^{15}$ cm^{-3}), various collisional effects can be important (see discussion in paper I).

The NS approach allows one to calculate (neglecting the collisional effects) the dielectronic recombination coefficients for the effective (direct plus cascade) transitions to the terminating levels i. The terminating levels are the metastable levels at which the cascades (originated from the autoionizing levels) terminate, that is, the probability of further downward radiative transitions is negligible. The effective dielectronic recombination coefficient α_i^D is defined in such a way that the rate of population (resulting from dielectronic recombination only) per unit volume and unit time, of the ith terminating level, is given by

TABLE VI. Magnetic dipole ($M1$) plus electric quadrupole ($E2$) lines (the "difficult" transitions) in the oxygen atom. λ_{ji} and A_{ji} are the line wavelength and Einstein's coefficient, respectively. The oscillator strengths f_{ij} for all the transitions are assumed to be equal to 10^{-9}.

$j\rightarrow i$	Transition	λ_{ji} (Å)	A_{ji} (s^{-1})
$4\rightarrow 2$	$2p^3 3s\,{}^5S^\circ\rightarrow 2p^4\,{}^1D$	1728.2	2.23
$6\rightarrow 2$	$2p^3 3p\,{}^5P\rightarrow 2p^4\,{}^1D$	1414.2	1.11
$8\rightarrow 2$	$2p^3 4s\,{}^5S^\circ\rightarrow 2p^4\,{}^1D$	1256.9	4.22
$4\rightarrow 3$	$2p^3 3s\,{}^5S^\circ\rightarrow 2p^4\,{}^1S$	2503.4	2.13×10^{-1}
$6\rightarrow 3$	$2p^3 3p\,{}^5P\rightarrow 2p^4\,{}^1S$	1894.2	1.24×10^{-1}
$8\rightarrow 3$	$2p^3 4s\,{}^5S^\circ\rightarrow 2p^4\,{}^1S$	1622.3	5.07×10^{-1}

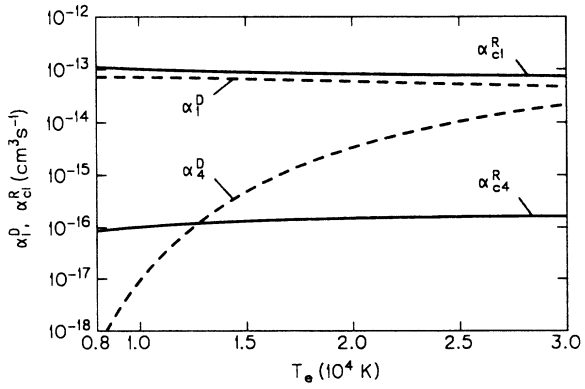

FIG. 5. T_e dependence of the effective dielectronic recombination rates α_i^D (dashed lines) and radiative recombination rates α_{ci}^R (solid lines) obtained in the present work.

TABLE VII. Constants in the effective dielectronic recombination rate coefficients α_i^D.

i	a	b	c	d	f
1	0.0051	0.0012	0.1377	−0.0135	0.6061
4	0.9887	−2.1047	3.6416	−0.2442	12.4049

$$\frac{dN_i^D}{dt}=N_eN_+\alpha_i^D\langle\kappa_{ai}\rangle\ , \tag{47}$$

and similarly,

$$\frac{dN_e^D}{dt}=-\sum_i N_eN_+\alpha_i^D\langle\kappa_{ai}\rangle\ , \tag{48}$$

and these terms are included in the rate equations (12) and (13) when $i=1$ and 4. Here,[50]

$$\alpha_i^D=10^{-12}(a/t+b+ct+dt^2)t^{-3/2} \times\exp(-f/t)\ \mathrm{cm^3\,s^{-1}}\ , \tag{49}$$

where $t=T_e(K)/10\,000$ K and the constants for the $i=1$ and 4 levels are listed in Table VII. The dielectronic rates α_1^D and α_4^D are compared with the radiative recombination rates α_{c1}^R and α_{c4}^R in Fig. 5. The radiative recombination rates are more important than the dielectronic recombination rates over the range of T_e considered here and this is opposite to the situation in atomic nitrogen (see paper I).

IX. RADIATIVE RECOMBINATION

Photoionization cross sections for oxygen atom can be obtained from the quantum-defect approach of Peach.[54–56] The quantum-defect photoionization cross section for a $L_pS_pnl\ LS\rightarrow L_pS_p\varepsilon'l'L'S$ transition is

$$\sigma_{ic}(\nu)=\frac{5.45\times10^{-19}n_{\mathrm{eff}}^3}{(1+\varepsilon'n_{\mathrm{eff}}^2)^3} \times\sum_{l'=l\pm1}C_{l'}\|G(n_{\mathrm{eff}}l;\varepsilon'l')\cos\Phi\|^2\ \mathrm{cm^2}\ , \tag{50}$$

with

$$\Phi=\pi[n_{\mathrm{eff}}+\mu_{l'}(\varepsilon')+\chi(n_{\mathrm{eff}}l;\varepsilon'l')]\ , \tag{51}$$

where $n_{\mathrm{eff}}=(\mathcal{R}/U_i)^{1/2}$ is the effective principle quantum number for the ith level and the ejected electron energy $\varepsilon'=h\nu-U_i$ is given in rydbergs. $\mu_{l'}(\varepsilon')$ is the quantum defect of the $l'L'$ series and it may be extrapolated to positive energy in the continuum spectrum as $\mu_{l'}(0)+b\varepsilon'$.[54,57] The values of the functions $G(n_{\mathrm{eff}}l;\varepsilon'l')$ $\chi(n_{\mathrm{eff}}l;\varepsilon'l')$ were calculated by Peach.[55] The values of $\mu_{l'}(0)$ and the slope b of the $l'L'$ series were obtained from Ref. 54 and they are summarized in Table VIII. The coefficient $C_{l'}$ in Eq. (50) is

$$C_{l'}=\sum_{L'=L\pm1}(2L'+1)\begin{Bmatrix} l & L & L_p \\ L' & l' & 1\end{Bmatrix}^2 l_{\max}\ , \tag{52}$$

where $l_{\max}$ is the larger of the two numbers l and l'.

In case of photoionization from the ground state, we use the simple but accurate approach of Henry[58]

$$\sigma_{ic}(\nu)=10^{-18}\sigma_{\mathrm{th}} \times\left[\alpha\left[\frac{\nu}{\nu_{\mathrm{th}}}\right]^{-s} +(1-\alpha)\left[\frac{\nu}{\nu_{\mathrm{th}}}\right]^{-(s+1)}\right]\ \mathrm{cm^2}\ , \tag{53}$$

where the photon frequency ν and the threshold frequency ν_{th} are

$$\nu=\frac{U_i+\varepsilon'}{h},\quad \nu_{\mathrm{th}}=\frac{U_i}{h}\ . \tag{54}$$

The parameters σ_{th}, α, and s for the photoionization from the atomic oxygen ground state are 2.94, 2.661, and 1, respectively. Once the photoionization cross section $\sigma_{ic}(\nu)$ is evaluated, the photorecombination cross section is calculated by using the Milne's relation (see paper I).

TABLE VIII. Quantum-defect parameters $\mu_{l'}(\varepsilon')$ for the $l'SL'$ series.

l'	$2S+1$	L'	$\mu_{l'}(0)$	b
0	3	0	1.150	−0.082
0	5	0	1.224	−0.088
1	3	1	0.711	−0.010
1	5	1	0.785	−0.190
2	3	2	0.024	0.051
2	5	2	0.040	0.110

X. RADIATION ESCAPE FACTORS

The radiation escape factors κ_{ji}, $\langle\kappa_{ai}\rangle$, and κ_{ci} of spectral, dielectronic, and continuum lines, respectively, are calculated in the way discussed in paper I. The escape factors κ_{ji} and $\langle\kappa_{ai}\rangle$ are calculated using the approach of Otsuka, Ikee, and Ishii.[59,60] At large optical depth $\langle\tau\rangle$, the functional dependence of the escape factors agrees with the asymptotic result of Holstein.[61]

XI. LINE INTENSITIES

The spectral line intensity is defined here as the net power radiated in all directions from a unit plasma volume located at the center of the plasma slab, whereas the continuum emission is specified in terms of the net power radiated per unit plasma volume, per unit solid angle, and per unit frequency range.

The intensity of the $j\rightarrow i$ spectral line in a homogeneous plasma is

$$I_{ji}=N_j A_{ji}\kappa_{ji} h\nu_{ji} \ . \tag{55}$$

The intensity of radiation produced by dielectronic recombination to a terminating level i (see paper I) is

$$I_i^D=N_e N_+ \alpha_i^D \langle h\nu_{ai}\rangle \langle \kappa_{ai}\rangle \ , \tag{56}$$

where $\langle h\nu_{ai}\rangle$ is the average energy of the photons emitted in the $a\rightarrow i$ transitions and $\langle \kappa_{ai}\rangle$ is the effective escape factor for these transitions. The autoionizing levels participating in populating of the terminating levels are spread over a certain interval of energy. Therefore the average photon energies $\langle h\nu_{ai}\rangle$ are taken as weighted averages

$$\langle h\nu_{ai}\rangle = \sum_a g_a(E_a-E_i)/\sum_a g_a \ , \tag{57}$$

where E_a and g_a are energy and statistical weight, respectively, of the ath autoionizing level. The sums in Eq. (57) are taken over all the autoionizing levels available for recombination to the ith terminating level.

The emission coefficients[62] for the free-bound and free-free continuum radiation in units of W cm^{-3} sr^{-1} s are, respectively,

$$j_\nu^{f\text{-}b}(\nu)=10^{-7}\sum_{i=1}^{\infty}\frac{h(2\nu a_0)^3}{c^2}\left[\frac{\pi\mathcal{R}}{kT_e}\right]^{3/2}\sigma_{ic}(\nu)\kappa_{ci}\frac{g_i}{g_+} \times N_e N_+ \exp\left[-\frac{h\nu-(U_i-\Delta E_\infty)}{kT_e}\right] , \tag{58}$$

and

$$j_\nu^{f\text{-}f}(\nu)=\frac{5.44\times10^{-46}G_{f\text{-}f}(\nu,T_e)z^2N_eN_+\exp(-h\nu/kT_e)}{T_e^{1/2}}[1+D(\nu,T_e)] \ . \tag{59}$$

The lowering of the ionization energies in a high-density plasma is estimated as[62]

$$\Delta E_\infty=\frac{ze^2}{\rho_D} \ , \tag{60}$$

where Debye radius in a singly ionized plasma is

$$\rho_D=\left[\frac{kT_e}{4\pi e^2(N_e+N_+)}\right]^{1/2} \ . \tag{61}$$

It may be added that the production (destruction) of negative ions does not contribute to the ΔE_∞ since the number of free charges in the plasma remains the same throughout the attachment (detachment) processes. In the emission frequency and electron temperature ranges considered in this work, the Gaunt factor is close to unity.[63] The correction factor $D(\nu,T_e)$ for the nonhydrogenic effect was evaluated by Asinovskii, Kirillin, and Kobsev,[64] giving

$$D(\nu,T_e)=-0.084-0.0182(1.3-T_e) -0.145\sin(0.6898\nu) \ , \tag{62}$$

where T_e and ν are given in units of 10^4 K and 10^4 cm^{-1}, respectively.

To compare the predicted total continuum emission with the measurements in high-pressure arc experiments,[65] one should consider the negative ion emission, which can be given by

$$j_\nu^-(\nu)=10^{-7}\sigma_{h\nu,\mathrm{det}}^{\mathrm{tot}}(\nu)N_-(T_e)B_\nu(T_e) \times[1-\exp(-h\nu/kT_e)] \ \mathrm{W\,cm^{-3}\,sr^{-1}\,s} \ , \tag{63}$$

where

$$B_\nu(T_e)=\frac{2h\nu^3/c^2}{\exp(h\nu/kT_e)-1} \ , \tag{64}$$

and $\sigma_{h\nu,\mathrm{det}}^{\mathrm{tot}}(\nu)$ is the total cross section for photodetachment of the negative ion (the photodetachment cross section is taken from the experimental measurements of Branscomb[2]). The density of the negative $O^-(^2P)$ ions is calculated from Eq. (18) by using the experimental value of $U_-=1.465$ eV and taking g_- as the statistical weight of the ground ionic state $O^-(^2P_{1/2,3/2})$.

The total intensity of the bound-bound spectral lines ($I_{b\text{-}b}$) is obtained by summing over all possible $j\rightarrow i$ transitions and the total intensity produced in the dielectronic recombination, (I_{di}) to all terminating levels is taken from the sum over $i=1$ and 4 levels. The power emitted in all directions per unit volume due to the free-bound, free-free, and negative-ion emission ($I_{f\text{-}b}$, $I_{f\text{-}f}$, and I_-, respectively) is calculated by multiplying the corresponding emission coefficient by $4\pi d\nu$ and integrating over all possible frequencies ν (see paper I). Then, the total intensity of radiation produced in the plasma is taken as a sum of spectral, dielectronic and continuum radiation, that is,

$$I_{\mathrm{tot}}=I_{b\text{-}b}+I_{\mathrm{di}}+I_{f\text{-}b}+I_{f\text{-}f}+I_- \ . \tag{65}$$

The intensity of radiation emitted per unit solid angle from 1 cm$\times$1cm$\times L$ column across plasma slab of thickness L is

$$I_{\mathrm{rad}}^L=\frac{I_{\mathrm{rad}}L}{4\pi} \ . \tag{66}$$

The radiation intensities discussed above are compared below with the blackbody radiation intensity, in W cm^{-2} sr,

$$I_P^L=10^{-7}\int_0^\infty B_\nu(T_e)d\nu=10^{-7}\frac{2(\pi kT_e)^4}{15c^2h^3} \ . \tag{67}$$

XII. RELAXATION TIMES

When the population of an atomic level departs (as a result of a small change of plasma parameters) from its steady-state value, then some time τ (called the relaxation time) is needed to reestablish steady-state distribution of the level. The relaxation times for each atomic oxygen

TABLE IX. Relaxation times (in sec) for levels $i=1,2,4,5,8$ of atomic oxygen.

T_e (K)	N_e (cm^{-3})	$i=1$	$i=2$	$i=4$	$i=5$	$i=8$
11 000	10^{10}	3.5×10^{-1}	2.4×10^{-2}	7.4×10^{-5}	5.0×10^{-9}	3.8×10^{-8}
	10^{13}	3.5×10^{-4}	2.4×10^{-5}	1.3×10^{-7}	4.6×10^{-9}	1.3×10^{-8}
	10^{16}	3.5×10^{-7}	2.4×10^{-8}	1.3×10^{-10}	6.1×10^{-11}	2.0×10^{-11}
13 000	10^{10}	2.1×10^{-1}	2.0×10^{-2}	6.9×10^{-5}	5.0×10^{-9}	3.8×10^{-8}
	10^{13}	2.1×10^{-4}	2.0×10^{-5}	1.1×10^{-7}	4.6×10^{-9}	1.3×10^{-8}
	10^{16}	2.1×10^{-7}	2.0×10^{-8}	1.1×10^{-10}	5.9×10^{-11}	2.1×10^{-11}
15 000	10^{10}	1.5×10^{-1}	1.7×10^{-2}	6.5×10^{-5}	5.0×10^{-9}	3.8×10^{-8}
	10^{13}	1.5×10^{-4}	1.7×10^{-5}	1.1×10^{-7}	4.6×10^{-9}	1.4×10^{-8}
	10^{16}	1.5×10^{-7}	1.7×10^{-8}	1.1×10^{-10}	5.6×10^{-11}	2.1×10^{-11}

level can be calculated in the way described in paper I. These times are given in Table IX. Due to lack of radiative coupling (but presence of strong collisional coupling) between the two lowest metastable levels ($i=2,3$) and the ground state, the relaxation time for the ground state of atomic oxygen is much shorter than, for example, that of the ground state of hydrogen.

As can be seen from the table, the relaxation times for the excited atoms are quite short, except at low electron densities ($N_e \lesssim 10^{10}$ cm^{-3}). Thus the quasisteady approximation (see discussion in paper I) can be used for description of nonstationary atomic oxygen under most of the conditions considered in this work. In other words, the system of the time-dependent rate equations for populations of the atomic levels in nonstationary atomic oxygen plasma can be solved assuming that all the excited levels are in steady state while the ground atomic level is in a transient state.

XIII. RESULTS AND DISCUSSION

Most of the results of this work are presented as a function of the electron temperature T_e and the total particle density N_t (see discussion in paper I). The density N_t is the total density of the plasma particles (bound and free) considered in the model, i.e.,

$$N_t = 2N_a + N_+ + N_e + 3N_- , \tag{68}$$

where $N_a = \sum_i N_i$ is the total density of all atoms in the gas and N_+, N_e, and N_- are positive ion, electron, and negative-ion densities (the ions are in the ground states), respectively. Under the conditions considered in this work, presence of positive ions with higher ionization degrees can be neglected. This and the assumption that the plasma is electrically neutral imply that the total density of the free charged particles is $N_+ + N_e$ while the total density of the charged particles bound in atomic species is equal to $2N_a$ [one electron and one ion (the atomic core)] and the number of charged particles bound in the negative ions is $3N_-$ (two electrons and one core). It should be emphasized that T_e and N_t are the two natural independent parameters of the steady-state plasma with no applied fields. Each set of these two parameters *uniquely* specifies the nonequilibrium properties of the stationary plasma; all the other microscopic properties, including N_e, depend on the values of T_e and N_t (see discussion in paper I).

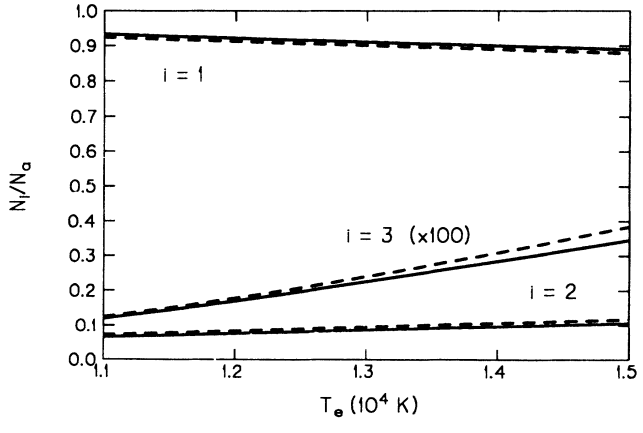

FIG. 6. Densities N_i of oxygen atoms in the ground state ($i=1$), in the first excited ($i=2$), and in the second excited ($i=3$) levels. N_a is the atomic density and T_e is the electron temperature. The total particle densities N_t are 10^{12} cm^{-3} (solid lines) and 10^{18} cm^{-3} (dashed lines).

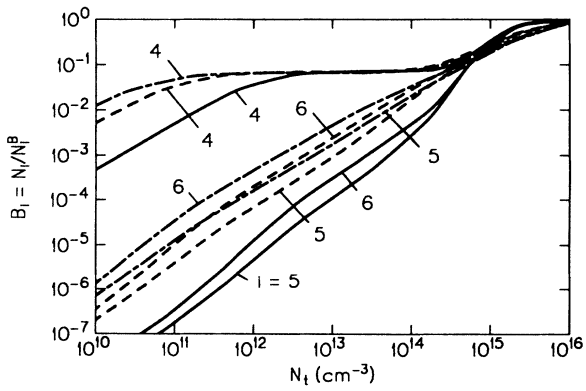

FIG. 7. Populations (coefficients B_i) of oxygen atoms excited to the $i=4$, 5, and 6 levels. N_t is the total particle density. The electron temperatures are 11 000 K (solid lines), 13 000 K (dashed lines), and 15 000 K (dot-dashed lines).

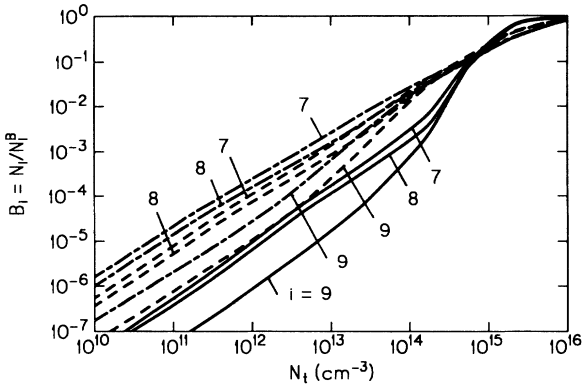

FIG. 8. Populations (coefficients B_i) of oxygen atoms excited to the $i=7$, 8, and 9 levels. N_t is the total particle density. The electron temperatures are 11 000 K (solid lines), 13 000 K (dashed lines), and 15 000 K (dot-dashed lines).

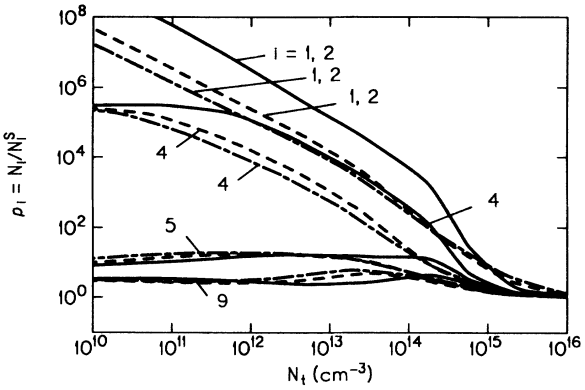

FIG. 10. Populations (coefficients ρ_i) of oxygen atoms excited to $i=1$, 2, 4, 5, and 9 levels. N_t is the total particle density. The electron temperatures are 11 000 K (solid lines), 13 000 K (dashed lines), and 15 000 K (dot-dashed lines).

The range of plasma density and temperature chosen in our calculations is limited by the following assumptions: (1) the atom-atom inelastic collisions do not contribute to the properties of the plasma, and (2) the role of doubly ionized atoms and excited singly ionized ions is negligible. The first assumption requires that $T_e \gtrsim 11\,000$ K while the second is justified if $N_e/N_a \ll 1$ ($T_e \lesssim 15\,000$ K).

Numerical calculations show that the atoms excited to the $i=2$ level are in the Boltzmann equilibrium with the ground-state atoms in the entire range of conditions considered here. In addition, the population of the atoms excited to this level is not far from the population of the ground-state atoms (Fig. 6). Population of the level $i=3$ is also relatively high and close to the Boltzmann equilibrium with the ground and first excited levels under most of the conditions. This is due to the lack of radiative coupling of the metastable levels $i=2$ and 3 with the ground state and the relatively small energy gaps between the levels (Fig. 1). However, at high T_e, the collisional coupling of these two levels with the upper excited levels and the continuum get stronger. Then the population of the level $i=3$ deviates slightly from the equilibrium values. The fact that the fraction of the atoms excited to the $i=2$ and 3 levels is large is important for the redistribution of energy in the plasma and for the plasma transport properties (the electrical and thermal conductivity, electron mobility, etc.). These properties depend on the cross sections for electron-atom elastic scattering; the cross sections are much greater for scattering by the excited atoms than for scattering by the ground-state atoms.

The populations of the upper electronic levels are given in Figs. 7 and 8. In Fig. 9, we show the N_e dependence of the ratios B_i in order to emphasize their weaker, than that of the functions $B_i(N_t, T_e)$, dependence on T_e. Populations of the upper levels in the atomic oxygen plasma show similar behavior as the upper levels in the atomic nitrogen plasma (paper I), except for the $i=4$ metastable level (Figs. 7 and 9). At low and medium densities the populations show almost linear N_t dependence. At high density the populations reach Boltzmann equilibrium

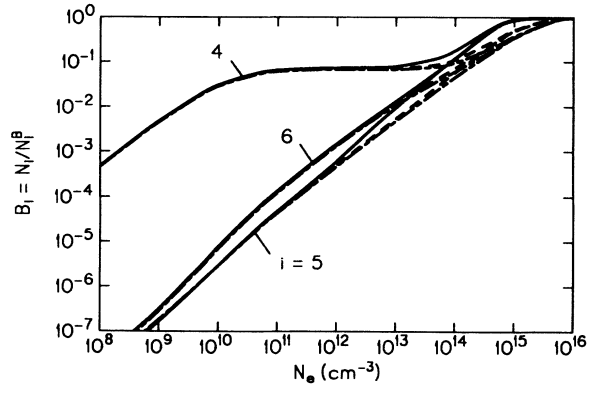

FIG. 9. Populations (coefficients B_i) of oxygen atoms excited to the $i=4$, 5, and 6 levels. N_e is the electron density. The electron temperatures are 11 000 K (solid lines), 13 000 K (dashed lines), and 15 000 K (dot-dashed lines).

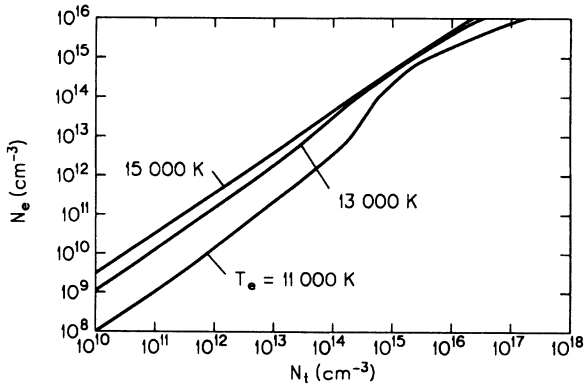

FIG. 11. Production of electrons in the atomic oxygen plasma as a function of the particle density N_t and electron temperature T_e.

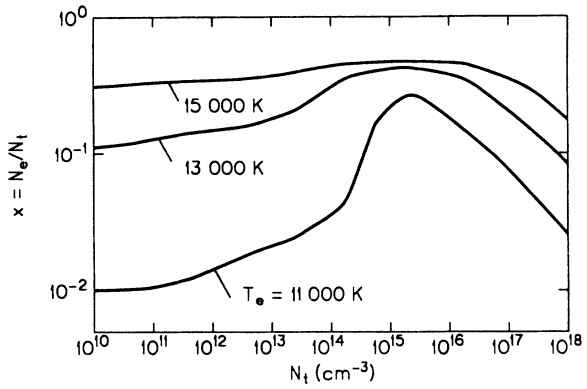

FIG. 12. Ionization degree $x = N_e/N_t$ of the atomic oxygen plasma as function of the particle density N_t and electron temperature T_e.

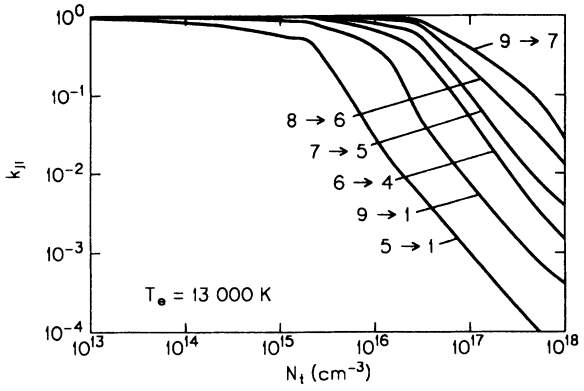

FIG. 14. N_t dependence of the radiation escape factors κ_{ji} for the 5→1, 9→1, 6→4, 7→5, 8→6, and 9→7 electric-dipole-allowed lines in the atomic oxygen plasma. The electron temperature is 13 000 K.

rapidly due to the increase in efficiency of both the collisional processes and the reabsorption of radiation in the plasma.

The kinetics of the $i = 4$ level, at a given T_e, can be discussed in conjunction with Figs. 7 and 9. The electron density range covered in Fig. 9 can be divided into three intervals. At $N_e \lesssim 10^{10}$ cm^{-3}, the electron density is low and the radiative terms $\sum_{j>4}^{n_{max}} B_j F_j A_{ji} \kappa_{ji}$ and the collisional terms $\sum_{k<4} N_e B_k F_k C_{k4}$ in Eq. (24) dominate the other terms and they are linear function of N_e. (Note that in this region of the electron density B_j is proportional to N_e and the first term in the numerator is also linear function of N_e since all the lower levels ($i = 1,2,3$) are close to Boltzmann equilibrium.) Equation (25) is dominated by the $\sum_{k<4} F_4 A_{4k} \kappa_{4k}$ terms which are independent of N_e. As a result, the coefficient B_4 increases linearly with electron density. At densities where 10^{10} cm$^{-3} \lesssim N_e \lesssim 10^{13}$ cm^{-3}, the collisional terms $\sum_{j>4}^{n_{max}} N_e F_4 C_{4j}$ become more important (due to the strong collisional coupling of the level 4 with the upper levels)

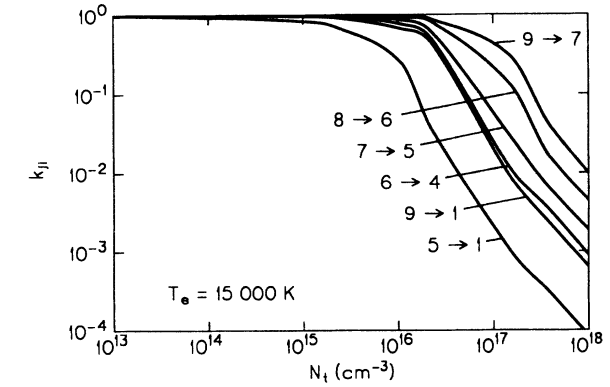

FIG. 15. N_t dependence of the radiation escape factors κ_{ji} for the 5→1, 9→1, 6→4, 7→5, 8→6, and 9→7 electric-dipole-allowed lines in the atomic oxygen plasma. The electron temperature is 15 000 K.

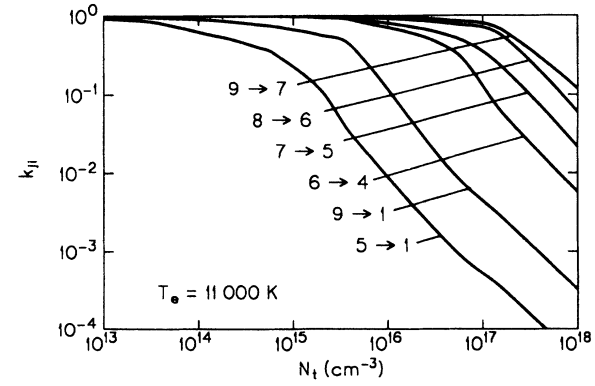

FIG. 13. N_t dependence of the radiation escape factors κ_{ji} for the 5→1, 9→1, 6→4, 7→5, 8→6, and 9→7 electric-dipole-allowed lines in the atomic oxygen plasma. The electron temperature is 11 000 K.

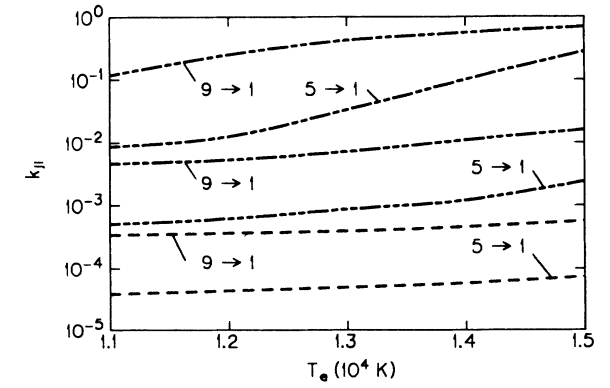

FIG. 16. T_e dependence of the radiation escape factors κ_{ji} for the 5→1 and 9→1 electric-dipole-allowed lines in the atomic oxygen plasma. The total particle densities N_t are 10^{16} cm^{-3} (–·–lines), 10^{17} cm^{-3} (– · · · –lines), and 10^{18} cm^{-3} (dashed lines).

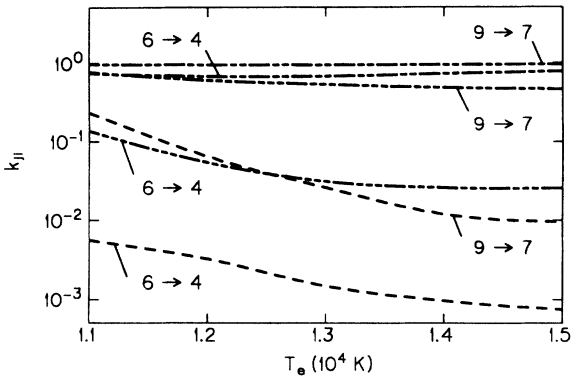

FIG. 17. T_e dependence of the radiation escape factors κ_{ji} for the 6→4 and 9→7 electric-dipole-allowed lines in the atomic oxygen plasma. The total particle densities N_t are 10^{16} cm^{-3} (–··–lines), 10^{17} cm^{-3} (– · · · –lines), and 10^{18} cm^{-3} (dashed lines).

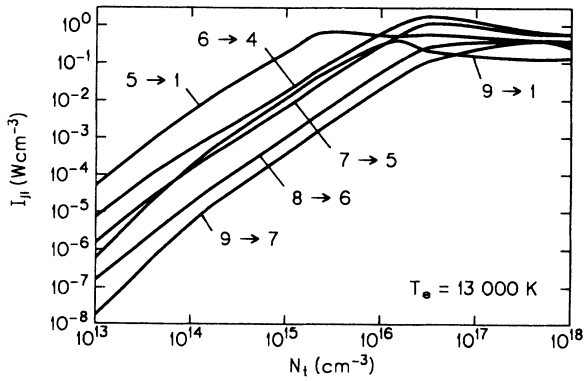

FIG. 19. N_t dependence of the line intensities I_{ji} for the 5→1, 9→1, 6→4, 7→5, 8→6, and 9→7 electric-dipole-allowed lines in the atomic oxygen plasma. The electron temperature is 13 000 K.

than the other terms in Eq. (25), and they are linearly dependent on N_e. Meanwhile, Eq. (24) is still dominated by the collisional terms $\sum_{k<4} N_e B_k F_k C_{k4}$ and the radiative terms $\sum_{j>4}^{n\max} B_j F_j A_{ji} \kappa_{ji}$. Hence B_4 is weakly dependent on the electron density. An increase of the electron density above 10^{13} cm^{-3} causes that the efficiency of the electron-impact collisions and the reabsorption of radiation in the plasma increase rapidly. Then the values of B_j become close to 1 and collisional coupling of the level 4 with all the upper levels is the dominating process. The terms $\sum_{j>4}^{n\max} N_e B_j F_j R_{j4}$ in Eq. (24) and the terms $\sum_{k<4} N_e B_k F_k C_{k4}$ in Eq. (25) are balancing each other. Then, the value of B_4 approaches 1.

The ratios ρ_i for several levels are shown in Fig. 10. As expected, the lowest three levels and the metastable level $i=4$ are far from Saha equilibrium at all temperatures, at low and medium densities, because their populations are controlled by the collisions involving the levels. The upper levels ($i \geq 5$) are close to each other and to continuum. Therefore their departure from Saha equilibrium is always smaller than that of the levels $i=1,2,3$, and 4. As the plasma density increases, all the levels approach collisional Saha-Boltzmann equilibrium.

The production of electrons in the atomic oxygen plasma is shown, as a function of T_e and N_t, in Figs. 11 and 12. One can see from there that the population of electrons is quite high in the entire considered range of conditions. This is due to the fact that the lowest metastable levels ($i=2,3,4$) contribute significantly to ionization of the gas. The ionization degree ($x=N_e/N_t$) increases significantly when N_t approaches values of 10^{15}–10^{16} cm^{-3}. Then, the number of atoms absorbing the radiation is large enough to cause strong reabsorption of radiation. This further enhances the efficiency of direct and stepwise ionization. At higher N_t, the population of electrons reaches the Saha equilibrium.

The escape factors κ_{ji} were calculated by assuming the width of the plasma slab $L=4$ cm and the atomic temperature $T_a=T_e$ (see discussion in paper I). The N_t dependence of the escape factors κ_{ji} for electric-dipole-

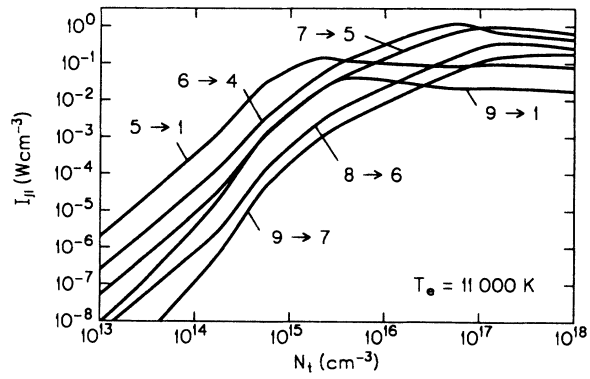

FIG. 18. N_t dependence of the line intensities I_{ji} for the 5→1, 9→1, 6→4, 7→5, 8→6, and 9→7 electric-dipole-allowed lines in the atomic oxygen plasma. The electron temperature is 11 000 K.

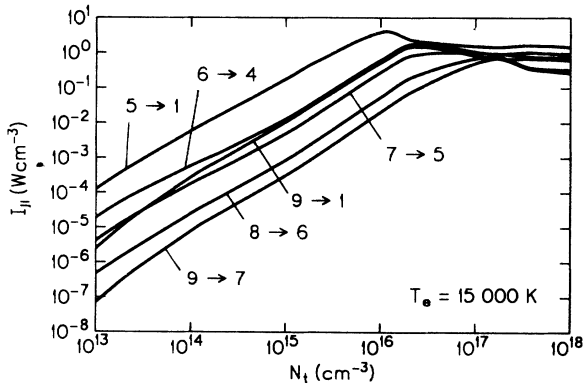

FIG. 20. N_t dependence of the line intensities I_{ji} for the 5→1, 9→1, 6→4, 7→5, 8→6, and 9→7 electric-dipole-allowed lines in the atomic oxygen plasma. The electron temperature is 15 000 K.

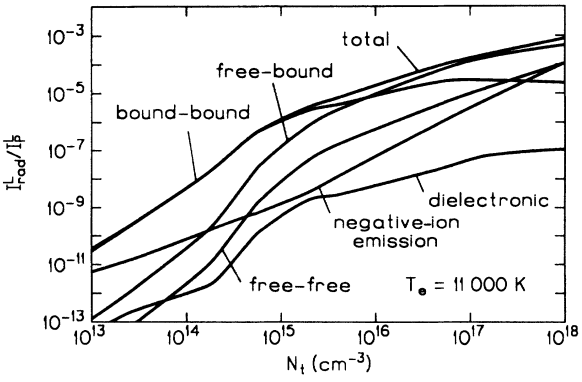

FIG. 21. N_t dependence of the ratios of the bound-bound ($I^L_{b\text{-}b}$), dielectronic (I^L_{di}), free-bound ($I^L_{f\text{-}b}$), free-free ($I^L_{f\text{-}f}$), negative-ion (I^L_-), and the total radiation intensity (I^L_{tot}) to the Planck (blackbody) intensity (I^L_P) in the atomic oxygen plasma. $I^L_{rad}=I_{rad}L/4\pi$ and $L=4$ cm. The electron temperature is 11 000 K.

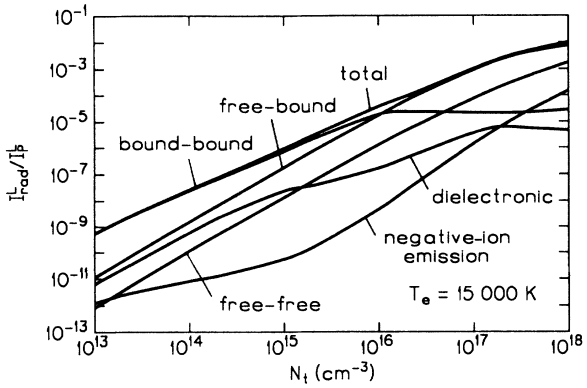

FIG. 23. N_t dependence of the ratios of the bound-bound ($I^L_{b\text{-}b}$), dielectronic (I^L_{di}), free-bound ($I^L_{f\text{-}b}$), free-free ($I^L_{f\text{-}f}$), negative-ion (I^L_-), and the total radiation intensity (I^L_{tot}) to the Planck (blackbody) intensity (I^L_P) in the atomic oxygen plasma. $I^L_{rad}=I_{rad}L/4\pi$ and $L=4$ cm. The electron temperature is 15 000 K.

allowed transitions is given in Figs. 13–15. The ability of the plasma to reabsorb the dipole-allowed lines increases monotonically with the plasma density. The T_e dependence of the escape factors for the $5\rightarrow1$ and $9\rightarrow1$ transitions is given in Fig. 16 and for the $6\rightarrow4$ and $9\rightarrow7$ transitions in Fig. 17. When the reabsorption involves the lowest three levels ($i=1,2,3$) as absorbers, the escape of radiation increases with T_e due to the decrease of the density of the absorbing levels through ionization and excitation to the upper excited levels. The escape of radiation produced by the dipole-allowed transitions to the levels with $i>3$ decreases when T_e increases because of the increasing number of the absorbing atoms produced by the excitation from the lowest three levels.

The intensities of several electric-dipole-allowed lines are shown in Figs. 18–20. At low and medium densities, these intensities increase almost linearly with N_t because of the almost linear increase in production of the upper radiative levels. At high densities the upper levels are in Boltzmann equilibrium with the ground state and in Saha equilibrium with the electrons. Then, the net production of the dipole-allowed radiation is density independent.

Various kinds of radiation produced in the atomic oxygen plasma are discussed in Figs. 21–23. At low and medium densities bound-bound radiation dominates the total plasma radiation. The dielectronic radiation is of several order of magnitude smaller than the free-bound radiation; this is quite different from the situations in atomic nitrogen (see paper I). At higher densities, the free-bound and free-free radiation become important, and at $T_e>13\,000$ K (higher ionization degrees) the latter radiation is dominant. Finally, one should note that the total plasma radiation is far from the blackbody emission even at high densities.

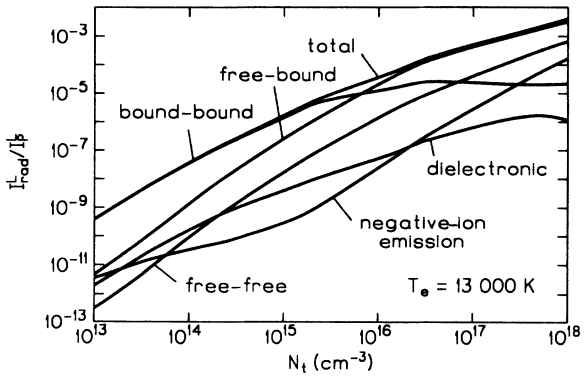

FIG. 22. N_t dependence of the ratios of the bound-bound ($I^L_{b\text{-}b}$), dielectronic (I^L_{di}), free-bound ($I^L_{f\text{-}b}$) free-free ($I^L_{f\text{-}f}$), negative-ion (I^L_-) and the total radiation intensity (I^L_{tot}) to the Planck (blackbody) intensity (I^L_P) in the atomic oxygen plasma. $I^L_{rad}=I_{rad}L/4\pi$ and $L=4$ cm. The electron temperature is 13 000 K.

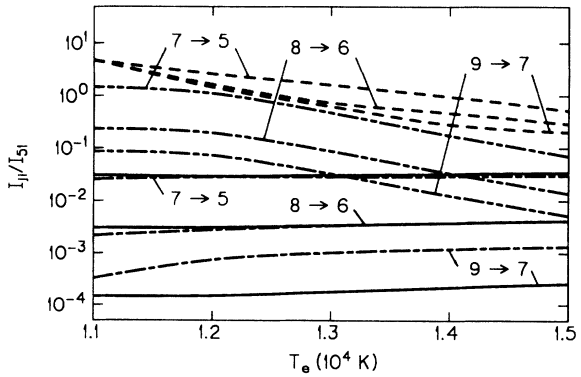

FIG. 24. T_e dependence of the line intensity ratios γ^{ji}_{51} of the dipole-allowed $7\rightarrow5$, $8\rightarrow6$, and $9\rightarrow7$ transitions to the dipole-allowed $5\rightarrow1$ transition in the atomic oxygen plasma with $N_t=10^{12}$ cm^{-3} (solid lines), 10^{14} cm^{-3} (dot-dashed lines), 10^{16} cm^{-3} (–·–line), and 10^{18} cm^{-3} (dashed line).

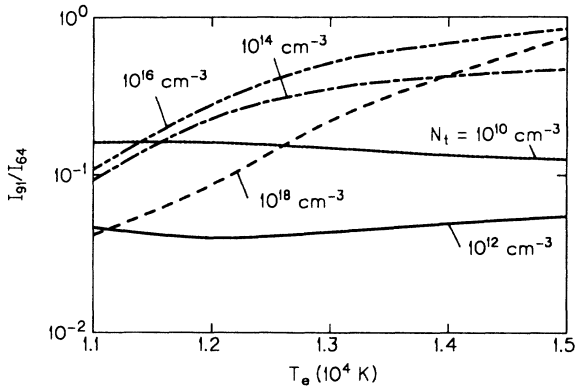

FIG. 25. T_e dependence of the line intensity ratio γ_{64}^{91} of the dipole-allowed $9 \rightarrow 1$ transition to the dipole-allowed $6 \rightarrow 4$ transition in the atomic oxygen plasma with $N_t = 10^{10}$ cm^{-3} (dotted line), 10^{12} cm^{-3} (solid line), 10^{14} cm^{-3} (dot-dashed line), 10^{16} cm^{-3} (–··–line), and 10^{18} cm^{-3} (dashed line).

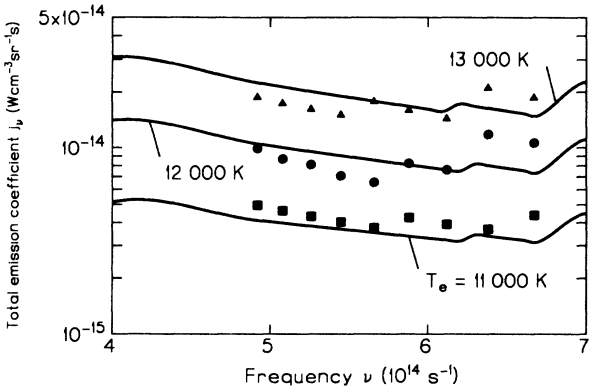

FIG. 27. Comparison of the calculated (solid lines) and measured total continuum emission coefficients $j_\nu = j_\nu^- + j_\nu^{f\text{-}b} + j_\nu^{f\text{-}f}$ for $T_e = 11\,000$ K (squares), 12 000 K (circles), 13 000 K (triangles), and $P = 1$ atm (Ref. 65).

T_e dependence of the intensity ratios of several dipole-allowed lines are given in Figs. 24 and 25. Some of the ratios can be used for diagnostics of the electron temperature but in a rather limited range. In situations when the weak emission of some of the forbidden lines is detectable, the ratios of the intensities of the electric-dipole-forbidden lines produced by the two lowest excited levels $i = 2$ and 3 to the intensities of some electric-dipole-allowed lines can be suitable for diagnostics of the plasma over a broader range of conditions. An example of a particularly useful choice of such ratio is given in Fig. 26.

Experimental work on microscopic properties of the high-temperature oxygen is very limited. The only existing data are the frequency-dependent measurements of the continuum radiation produced in high-density oxygen discharge.[65] The comparison of our results with the measured values of the total emission coefficient $j_\nu = j_\nu^- + j_\nu^{f\text{-}b} + j_\nu^{f\text{-}f}$ is given in Fig. 27. Since part of the measured continuum spectrum is in the low-frequency region, we calculated the total free-bound emission as a sum of radiation produced in the free-bound transitions to 24 atomic levels; levels with $i > 24$ are neglected since they only contribute at lower frequencies ($\nu \lesssim 5 \times 10^{14}$ s^{-1}) where the spectrum is dominated by the negative-ion emission. At high electron density, all the levels with $i > 9$ are close to Boltzmann equilibrium with each other and to Saha equilibrium with the electrons. The photoionization cross sections for levels $10 \leq i \leq 14$ are taken from the quantum-defect theory, while the hydrogenic photoionization cross sections are applied to the rest of the highly excited levels. [The hydrogenic cross sections can be used for photoionization of the highly excited levels because the quantum defects of these levels are close to zero. For zero quantum defect, Peach's quantum-defect (nonhydrogenic) cross sections converge to the hydrogenic formula.[54–56]]

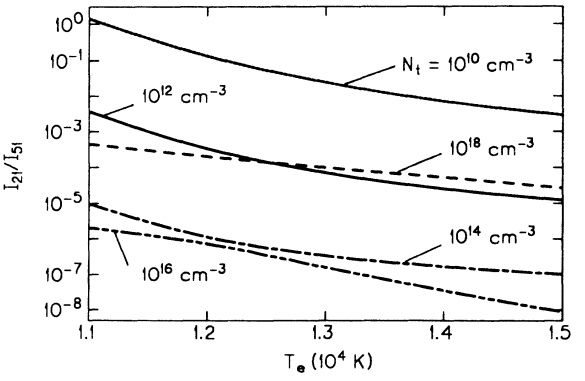

FIG. 26. T_e dependence of the line intensity ratio γ_{51}^{21} of the dipole-forbidden $2 \rightarrow 1$ transition to the dipole-allowed $5 \rightarrow 1$ transition in the atomic oxygen plasma with $N_t = 10^{10}$ cm^{-3} (dotted line), 10^{12} cm^{-3} (solid line), 10^{14} cm^{-3} (dot-dashed line), 10^{16} cm^{-3} (–··–line), and 10^{18} cm^{-3} (dashed line).

The present calculations show that the negative-ion emission is important in the frequency range of continuum radiation considered in the comparison ($U_- \leq h\nu \lesssim 3$ eV). For example, at $\nu = 6 \times 10^{14}$ s^{-1} (or $\lambda = 5000$ Å), the negative-ion emission is responsible for about 55% (when $T_e = 11\,000$ K) to 23% (when $T_e = 13\,000$ K) of the total continuum radiation produced by the oxygen plasma. Thus inclusion of the negative-ion continuum emission is necessary for correct interpretation of the mechanisms producing the continuum radiation is oxygen plasmas. As can be seen from Fig. 27, the agreement of the measured intensity of continuum radiation with the predictions of this work is very good.

In conclusion, one should add that the question of the influence of the inelastic cross sections accuracy on reliability of the solutions obtained from collisional-radiative models is still open; it will be possible to give a detail answer to this question when complete sets of precalculated, from an accurate method, cross sections are available. (It seems at present that the most promising initiative in this direction is the cooperative opacity program (see paper I), created originally for calculating radiative processes, which is now being modified to study

electron-atom and electron-ion inelastic collisions.) However, we made a partial study of the sensitivity of the kinetic model to different cross sections by comparing solutions obtained with two different sets of cross sections for the important $i = 1 \rightarrow 2,3,4,5,6,7$ electron-impact transitions. The first set of the cross sections was the one used in this work (all the cross sections were taken from the *reliable measurements* discussed above). The other set contained cross sections obtained from available *modern theoretical approaches* cited above. The solutions of the model using these two sets of the cross sections do not differ significantly; in the worst case (low densities) the maximum difference in the population of some levels was less than a factor of 5. This results from the fact that the modern methods of calculating of the cross sections give results that are not far from reality.

ACKNOWLEDGMENTS

The authors thank Alex Dalgarno and Verne Jacobs for valuable comments. This work was supported by the National Aeronautics and Space Administration, Grant No. NAGW-1061 and the Air Force Office of Scientific Research, Grant Nos. 88-0119 and 88-0146.

[1]J. A. Kunc and W. H. Soon, Phys. Rev. A **40**, 5822 (1989).
[2]L. M. Branscomb, in *Atomic and Molecular Processes,* edited by D. R. Bates (Academic, New York, 1962), p. 100.
[3]G. C. Tisone and L. M. Branscomb, Phys. Rev. **170**, 169 (1968).
[4]H. S. W. Massey, *Negative Ions* (Cambridge University Press, Cambridge, 1976).
[5]S. J. Smith, in *Proceedings of the Fourth International Conference on Ionization Phenomena in Gases, Uppsala, 1959,* edited by N. R. Nilsson (North-Holland, Amsterdam, 1960), p. 219.
[6]R. E. Olson, J. R. Peterson, and J. T. Moseley, J. Geophys. Res. **76**, 2516 (1971).
[7]R. E. Olson, J. R. Peterson, and J. T. Moseley, J. Chem. Phys. **53**, 3391 (1970).
[8]A. P. Hickman, J. Chem. Phys. **70**, 4872 (1979).
[9]I. I. Sobelman, L. A. Vainshtein, and E. A. Yukov, *Excitation of Atoms and Broadening of Spectral Lines* (Springer-Verlag, New York, 1981).
[10]I. I. Sobelman and L. A. Vainshtein, J. Quant. Spectrosc. Radiat. Transfer **8**, 1491 (1968).
[11]J. P. Doering and E. E. Gulcicek, J. Geophys. Res. **94**, 2733 (1989).
[12]J. P. Doering and E. E. Gulcicek, J. Geophys. Res. **94**, 1541 (1989).
[13]E. E. Gulcicek, J. P. Dering, and S. O. Vaughan, J. Geophys. Res. **93**, 5885 (1988).
[14]E. E. Gulcicek and J. P. Doering, J. Geophys. Res. **93**, 5879 (1988).
[15]S. O. Vaughan and J. P. Doering, J. Geophys. Res. **92**, 7749 (1987).
[16]S. O. Vaughan and J. P. Doering, J. Geophys. Res. **91**, 13755 (1986).
[17]E. C. Zipf and P. W. Erdman, J. Geophys. Res. **90**, 11087 (1985).
[18]P. S. Julienne and J. Davis, J. Geophys. Res. **81**, 1397 (1976).
[19]E. R. Smith, Phys. Rev. A **13**, 65 (1976).
[20]S. P. Rountree, J. Phys. B **10**, 2719 (1977).
[21]S. P. Rountree and R. J. W. Henry, Phys. Rev. A **6**, 2106 (1972).
[22]R. J. W. Henry, P. G. Burke, and A. L. Sinfailam, Phys. Rev. **178**, 218 (1969).
[23]V. K. Lan, N. Feautrier, M. L. Dourneuf, and H. V. Regemorter, J. Phys. B **5**, 1506 (1972).
[24]L. D. Thomas and R. K. Nesbet, Phys. Rev. A **11**, 170 (1975).
[25]K. Smith, R. J. W. Henry, and P. G. Burke, Phys. Rev. **157**, 51 (1967).
[26]K. Smith, M. J. Conneely, and L. A. Morgan, Phys. Rev. **177**, 177 (1969).
[27]M. J. Seaton, in *The Airglow and the Aurorae,* edited by E. B. Armstrong and A. Dalgarno (Pergamon, London, 1956), p. 289.
[28]T. Sawada and P. S. Ganas, Phys. Rev. A **7**, 617 (1973).
[29]T. W. Shyn and W. E. Sharp, J. Geophys. Res. **91**, 1691 (1986).
[30]T. W. Shyn, S. Y. Cho, and W. E. Sharp, J. Geophys. Res. **91**, 13751 (1986).
[31]L. Vriens, Phys. Rev. A **141**, 88 (1966).
[32]E. Brook, M. F. A. Harrison, and A. C. H. Smith, J. Phys. B **11**, 3115 (1978).
[33]E. C. Zipf, Planet. Space Sci. **33**, 1303 (1985).
[34]M. Gryzinski and J. A. Kunc, J. Phys. B **19**, 2479 (1986).
[35]R. H. Garstang, Proc. Cambridge Philos. Soc. **57**, 115 (1961).
[36]R. H. Garstang, Mon. Not. R. Astron. Soc. **111**, 115 (1951).
[37]C. Goldbach, M. Martin, G. Nollez, P. Plomdeur, J. P. Zimmermann, and D. Babic, Astron. Astrophys. **161**, 47 (1986).
[38]A. Hibbert, P. L. Dufton, and F. P. Keenan, Mon. Not. R. Astron. Soc. **213**, 721 (1985).
[39]M. W. Chang, Astrophys. J. **211**, 300 (1977).
[40]P. D. Dumont, E. Biemont, and N. Grevesse, J. Quant. Spectrosc. Radiat. Transfer **14**, 1127 (1974).
[41]A. K. Pradhan and H. E. Saraph, J. Phys. B **10**, 3365 (1977).
[42]C. J. Zeippen, M. J. Seaton, and D. C. Morton, Mon. Not. R. Astron. Soc. **181**, 527 (1977).
[43]D. B. Jenkins, J. Quant. Spectrosc. Radiat. Transfer **34**, 55 (1985).
[44]W. L. Wiese, M. W. Smith, and B. M. Glennon, *Atomic Transition Probabilities,* Natl. Bur. Stand. Ref. Data Ser., Natl. Bur. Stand. (U.S.) Circ. No. 4 (U.S. GPO, Washington, D.C., 1966), Vol. I.
[45]A. Omholt, Planet. Space Sci. **2**, 246 (1960).
[46]A. Omholt, Geofys. Publ. **21**, 1 (1959).
[47]R. H. Garstang, in *The Airglow and The Aurorae,* edited by E. B. Armstrong and A. Dalgarno (Pergamon, New York, 1956), p. 324.
[48]I. I. Sobelman, *Atomic Spectra and Radiative Transitions* (Springer, Berlin, 1979).
[49]E. Clementi and D. L. Raimondi, J. Chem. Phys. **38**, 2686 (1963).
[50]H. Nussbaumer and P. J. Storey, Astron. Astrophys. **126**, 75 (1983).
[51]H. Nussbaumer and P. J. Storey, Astron. Astrophys. Suppl. Ser. **56**, 293 (1984).
[52]A. Burgess, Astrophys. J. **139**, 776 (1964).
[53]R. H. Bell and M. J. Seaton, J. Phys. B **18**, 1589 (1985).
[54]G. Peach, Mem. R. Astron. Soc. **71**, 1 (1967).
[55]G. Peach, Mem. R. Astron. Soc. **71**, 13 (1967).
[56]G. Peach, Mem. R. Astron. Soc. **73**, 1 (1970).
[57]M. J. Seaton, Mon. Not. R. Astron. Soc. **118**, 504 (1958).
[58]R. J. Henry, Astrophys. J. **161**, 1153 (1970).
[59]M. Otsuka, J. Quant. Spectrosc. Radiat. Transfer **21**, 489

(1979).
[60]M. Otsuka, R. Ikee, and K. Ishii, J. Quant. Spectrosc. Radiat. Transfer **21**, 41 (1979).
[61]T. Holstein, Phys. Rev. **83**, 1159 (1951).
[62]H. R. Griem, *Plasma Spectroscopy* (McGraw-Hill, New York, 1964).
[63]G. B. Rybicki and A. P. Lightman, *Radiative Processes in Astrophysics* (Wiley, New York, 1979).
[64]Z. J. Asinovskii, A. V. Kirillin, and G. A. Kobsev, J. Quant. Spectrosc. Radiat. Transfer **10**, 143 (1970).
[65]G. Boldt, Z. Phys. **154**, 319 (1959).
[66]S. M. V. Aldrovandi and D. Pequignot, Astron. Astrophys. **25**, 137 (1973).
[67]J. M. Shull and M. van Steenberg, Astrophys. J. **48**, 95 (1982).